ELSEVIER

Journal of Computational and Applied Mathematics 109 (1999) 1–39

JOURNAL OF COMPUTATIONAL AND APPLIED MATHEMATICS

www.elsevier.nl/locate/cam

Inversion methods in helioseismology and solar tomography ☆

A.G. Kosovichev

W.W. Hansen Experimental Physics Laboratory, Stanford University, Stanford, CA 94305-4085, USA

Received 15 September 1998; received in revised form 9 March 1999

Abstract

Basic methods by which the internal structure and dynamics of the Sun can be inferred from observed frequencies of solar oscillations and acoustic travel times are discussed. The methods for inverting the oscillation frequencies are based on a variational formulation of the adiabatic eigenvalue problem for a star. The inversion technique formulated in terms of linear integral constraints provides estimates of localized averages of properties of the solar structure, such as density and sound speed, helium abundance in the convection zone for a given equation of state, and, in addition, the estimates for the internal rotation rate. The method of inverting acoustic travel times employs a geometrical ray approximation and provides 3D images of solar convective cells, active regions and sunspots. The information about the global and local structures and flow velocities in the solar interior is important for understanding solar evolution and mechanisms of solar activity. The high-resolution helioseismology projects from space provide a tremendous amount of data, the interpretation of which is increasingly challenging and requires the development of efficient inversion methods and algorithms.

Keywords: Inverse problems; Eigenvalues; Variational principle; Least-squares method; Tikhonov regularization; Backus–Gilbert method; Asymptotic approximation

1. Introduction

Helioseismology provides a unique tool to probe the internal structure and dynamics of a star. The information about the thermodynamic and magnetic properties and internal rotation and flows is obtained by inverting the frequencies and travel times of solar oscillations. This information is important for understanding the solar constitution and evolution, processes of the energy generation and transport, and mechanisms of the 22-year cycle of solar activity which affects Earth's space environment.

E-mail address: sasha@khors.stanford.edu (A.G. Kosovichev)

☆ Electronic Annex available. See http://www.elsevier.nl/locate/cam

0377-0427/99/$ - see front matter
PII: S0377-0427(99)00152-1

The Sun's interior consists of two main regions: the inner radiative zone where the solar energy is transported by radiation and the outer zone of convective energy transport which occupies approximately 30% of the solar radius. The upper convective boundary layer is believed to be the place where the solar oscillations are excited. The excitation mechanism is stochastic. Predominantly excited waves are acoustic and surface gravity waves with oscillation periods of 3–10 min in a wide range of wave numbers. The combined amplitude of the oscillations is about 200 $\mathrm{m\,s^{-1}}$.

The oscillations are usually observed on the solar surface by measuring the Doppler shift of solar absorption lines formed in the lower part of the solar atmosphere. There are numerous ground-based and space projects to observe solar oscillations. The most prominent projects are the GONG (Global Oscillation Network Group with six observing stations around the globe) [32] and the SOI-MDI (Solar Oscillation Investigation — Michelson Doppler Imager) on the space solar observatory SOHO [66]. The data from these experiments have provided detailed information about the internal structure and rotation of the Sun [29,48,68].

There are two basic approaches to infer solar properties from the oscillation data. The first approach is to study the resonant properties of the solar interior by determining the eigenfrequencies of the oscillations (e.g. [63]). The second approach is to measure and invert the wave travel times between different points on the surface [18]. Because of the stochastic nature of solar oscillations substantial spatial and temporal averaging of data is required to measure the frequencies and travel times accurately. The frequencies of solar eigenmodes are obtained from the oscillation power spectra, an example of which is shown in Fig. 1. The travel times are measured from cross-covariance of oscillation signals at different distances (Section 4). These two approaches are complementary: the first is mainly used to infer large-scale properties through the whole Sun, whereas the second has been useful for determining local properties of convective and magnetic structures in the subsurface layers.

In this review, I discuss the basic mathematical and computational techniques of helioseismology. Most of these techniques are based on a perturbation analysis which results in linear integral relations between the measured properties of solar oscillations (mode frequencies and travel times) and the interior properties of the Sun. The solar properties are then inferred by standard linear inversion techniques, e.g. by the regularized least-squares method [77] or by the optimally localized averaging technique [4]. The helioseismic inversions deal with large data sets which consist typically of 10^3–10^4 data points for the structure inversions, and of 10^5–10^6 data points for inversions for solar rotation and local properties. Therefore, the development of efficient methods and algorithms is very important in this field.

Solar p modes can be classified in terms of three integer parameters, which represent the spatial structure of their eigenfunctions. Degree l and azimuthal order m of the spherical harmonics describe the angular structure of the eigenfunctions, and integer n, called radial order, labels the modes according to their radial structure and normally is the number of nodes in the radial direction. For a spherically symmetric stellar model, the mode eigenfrequencies, ω_{nlm}, are degenerate with respect to m. Rotation and asphericity of the Sun break the symmetry. Therefore, the frequencies of different n and l are split into multiplets, in which the central frequency of $m = 0$ (zonal modes) represents the spherically symmetric component of the solar structure. The modes with nonzero m are shifted with respect to the central frequency. The frequency shift depends on the value of m and on solar rotation and other nonsymmetrical phenomena, like convection and magnetic field. In the first-order approximation, the average multiplet frequency is equal to the eigenfrequency of the zonal mode of $m=0$. The average frequencies are usually provided in helioseismic data, because those are estimated

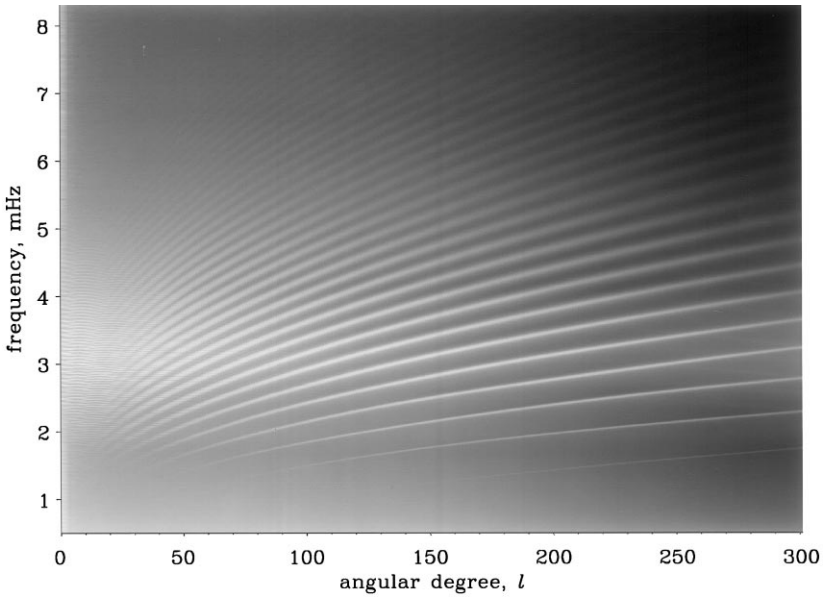

Fig. 1. Power spectrum (frequency-angular degree diagram) obtained from the MDI data [48]. The bright ridges show the oscillation power of solar modes: the lowest and weakest ridge corresponds to the fundamental mode of the Sun, the ridge above it represents the first acoustic mode, and the higher ridges are higher radial overtones of acoustic oscillations. The angular degree, l, is that of the spherical harmonic function describing the surface variation of the modal pattern. It is essentially a spatial wavenumber.

with better accuracy than the zonal-mode frequencies. However, in the second-order approximation there is a systematic shift between the average frequencies and corresponding eigenfrequencies of $m = 0$ modes. These shifts have to be taken into account when small-amplitude features of solar structure are studied [19].

Two approaches to solar structure inversions have been considered: an asymptotic technique, and a perturbation method based on a variational principle. Both methods are borrowed from geophysics. The asymptotic technique was originally developed by Brodsky and Levshin [8], and the variational method was employed by Backus and Gilbert [4] (for reviews of their helioseismic applications see [30,31]). The most obvious deficiency of the asymptotic technique is its lack of precision which is particularly poor in the zones of rapid variations of solar properties, such as the boundaries of the convection zone, ionization zones and subphotospheric layers [37]. The variational approach is based on the full oscillation equations, and, therefore, it permits to obtain more information from the data. Because of nonlinearity these equations can be solved by an iterative procedure like a generalized Newton–Raphson method.

A variational principle for the adiabatic oscillation eigenfrequencies, and differential kernels which measure sensitivity of frequencies to local perturbations of density ρ and specific heat ratio γ, are presented in Section 2.1. In Section 2.2, I describe a general method for computation of the differential kernels for other hydrostatic parameters, for example, for $u \equiv p/\rho$ and helium abundance, Y, using stellar structure equations and the equation of state. An inversion technique to estimate localized averages of solar parameters is given in Section 2.3. Some inversion results demonstrating resolution and accuracy of the inversion technique are presented in Section 2.4.

The methods and algorithms for inferring the rotation rate inside the Sun are described in Section 3, including a formulation of the forward problem (Section 3.1), a 2D asymptotic method based on Abel integral inversion (Section 3.2.1), and numerical methods (Sections 3.2.2 and 3.2.3). Some inversion results for the current helioseismic data are summarized in Section 3.4.

Solar tomography is reviewed in Section 4. This review includes methods of computing and interpreting acoustic travel times (Section 4.1), inversion methods (Section 4.2), and initial results (Section 4.3). In Section 5 some future directions for developing helioseismic inversion techniques and solar tomography are briefly discussed.

2. Inversions for the solar structure

2.1. Eigenvalue problem: variational principle for eigenfrequencies

The motions in a star in the simplest case with no heat sources and no heat exchange and extra forces (such as magnetic and Reynolds stress forces) are described by the hydrodynamic equations of conservation of mass, momentum, energy and by Poisson's equation

$$\frac{\partial \rho}{\partial t} + \operatorname{div}(\rho \boldsymbol{v}) = 0, \tag{1}$$

$$\rho\left(\frac{\partial \boldsymbol{v}}{\partial t} + \boldsymbol{v}\cdot\boldsymbol{\nabla}\boldsymbol{v}\right) = -\boldsymbol{\nabla}p - \rho\boldsymbol{\nabla}\Phi, \tag{2}$$

$$\frac{\partial S}{\partial t} + \boldsymbol{v}\cdot\boldsymbol{\nabla}S = 0, \tag{3}$$

$$\boldsymbol{\nabla}^2\Phi = 4\pi G\rho. \tag{4}$$

Here ρ, $\boldsymbol{v}$, p, Φ, T and S are the density, fluid velocity, pressure, gravitational potential, temperature and specific entropy, respectively, and G is the gravitational constant. These equations are complemented by the equation of state: $S = S(p,\rho)$, and boundary conditions of regularity at the star center.

Since the amplitude of solar oscillations is small they can be described in terms of small perturbations to a stationary equilibrium state which in the first approximation is a function of only radius r. The perturbation equations are

$$\frac{\partial \rho'}{\partial t} + \operatorname{div}(\rho \boldsymbol{v}') = 0, \tag{5}$$

$$\rho\frac{\partial \boldsymbol{v}'}{\partial t} = -\boldsymbol{\nabla}p' - \rho\boldsymbol{\nabla}\Phi' - \rho'\boldsymbol{\nabla}\Phi, \tag{6}$$

$$\frac{\partial p'}{\partial t} + \boldsymbol{v}'\cdot\boldsymbol{\nabla}p - \left(\frac{\partial p}{\partial \rho}\right)_S\left(\frac{\partial \rho'}{\partial t} + \boldsymbol{v}'\cdot\boldsymbol{\nabla}\rho\right) = 0, \tag{7}$$

$$\boldsymbol{\nabla}^2\Phi' = 4\pi G\rho', \tag{8}$$

where the variables without subscript denote properties of the equilibrium state, and the prime sign refers to small perturbations of the properties due to oscillations; $(\partial p/\partial\rho)_S \equiv c^2$ is the adiabatic sound speed, which is also represented in terms of the adiabatic exponent, $\gamma \equiv (\partial \log P/\partial \log \rho)_S$: $c^2 = \gamma P/\rho$.

The fourth-order system of equations (5)–(8) is complemented by boundary conditions describing regularity of the solution at the star center, $r = 0$, and the absence of external forces on the surface $r = R$. The oscillatory solution of this system has time dependence $\exp(\mathrm{i}\omega t)$, and can be expressed in terms of Fourier components of the fluid displacement, $\boldsymbol{\xi}$,

$$\boldsymbol{v}' = \partial\boldsymbol{\xi}/\partial t = \mathrm{i}\omega\boldsymbol{\xi}, \tag{9}$$

where ω in the oscillation frequency. As a result, we obtain an eigenvalue problem for a fourth-order system of ordinary linear differential equations. In this formulation, the eigenvalue problem is nonlinear in terms of the squared eigenfrequency, ω^2, and typically solved by iterations for a given initial equilibrium state.

The inverse problem of helioseismology is to estimate the properties of the equilibrium state from a set of observed eigenfrequencies. The standard approach to this problem is to find corrections to models of the equilibrium state which are sufficiently close to the real Sun, so that a perturbation theory can be employed.

Eqs. (5)–(9) together with the boundary conditions can also be represented in a linear operator form:

$$\mathscr{L}\boldsymbol{\xi} + \omega^2\boldsymbol{\xi} = 0, \tag{10}$$

where $\mathscr{L}$ is a self-adjoint integro-differential operator [13]. Therefore, the eigenfunctions $\boldsymbol{\xi}$ are orthogonal. Eigenvalues ω^2 are real and obey a variational principle [10]. For a normal mode, i, the variational principle gives an integral relation for the eigenfrequency, ω_i:

$$\omega_i^2 = W_i/I_i, \tag{11}$$

where

$$W_i = \int_V [\gamma p(\operatorname{div}\boldsymbol{\xi}_i)^2 + 2(\boldsymbol{\xi}_i\cdot\boldsymbol{\nabla}p)\operatorname{div}\boldsymbol{\xi}_i + \rho^{-1}(\boldsymbol{\xi}_i\cdot\boldsymbol{\nabla}\rho)(\boldsymbol{\xi}_i\cdot\boldsymbol{\nabla}p)]\,\mathrm{d}V$$
$$- G\int_V\int_V |\boldsymbol{r}_i - \boldsymbol{r}_i'|^{-1}\operatorname{div}[\rho\boldsymbol{\xi}_i]\operatorname{div}[\rho'\boldsymbol{\xi}_i']\,\mathrm{d}V\,\mathrm{d}V' \tag{12}$$

is a quantity proportional to the potential energy of the mode averaged over the period of the oscillation, and

$$I_i = \int_V \rho\boldsymbol{\xi}_i^2\,\mathrm{d}V \tag{13}$$

can be regarded as mode inertia. Here V is the star volume. Eq. (11) represents the balance between the potential and kinetic energies averaged over the period of the oscillation modes. In a spherically symmetric star, the displacement eigenfunctions, $\boldsymbol{\xi}_i$, can be expressed in terms of spherical harmonics $Y_{lm}(\theta,\phi)$:

$$\boldsymbol{\xi}_i(r,\theta,\phi) = \boldsymbol{e}_r\xi_i(r)Y_{lm}(\theta,\phi) + \eta_i(r)\boldsymbol{\nabla}_\perp Y_{lm}(\theta,\phi), \tag{14}$$

where $\xi_i(r)$ and $\eta_i(r)$ represent the radial dependence of the radial and horizontal components of the displacement vector, $\boldsymbol{\nabla}_\perp = \boldsymbol{e}_\theta(\partial/\partial\theta) + \boldsymbol{e}_\phi(1/\sin\theta)(\partial/\partial\phi)$ is the angular part of the gradient in spherical coordinates, (r,θ,ϕ), and $\boldsymbol{e}_r$, $\boldsymbol{e}_\theta$, $\boldsymbol{e}_\phi$ are units vectors in the directions of r, θ, ϕ.

Eqs. (12) and (13) can be written in term of ξ_i and η_i, and perturbation of the gravitational potential Φ' [3]:

$$W_i = 4\pi \int_0^R \gamma p \left(\frac{\mathrm{d}\xi_i}{\mathrm{d}r} + \frac{2\xi_i}{r} - \frac{l(l+1)\eta_i}{r} \right)^2 r^2 \,\mathrm{d}r + 4\pi \int_0^R \rho r^2 \left[-\frac{4}{r} g \xi_i^2 + \xi_i (g_i' + 4\pi G \rho \xi_i) + l(l+1) \frac{\eta_i}{r} (\Phi_i' + 2g\xi_i) \right] \mathrm{d}r, \tag{15}$$

$$I_i = 4\pi \int_0^R \rho r^2 [\xi_i^2 + l(l+1)\eta_i^2] \,\mathrm{d}r, \tag{16}$$

where

$$g' = \frac{\partial \Phi'}{\partial r}, \qquad \nabla^2 \Phi' = 4\pi G \rho', \qquad g = \frac{Gm}{r^2} \equiv \frac{4\pi G}{r^2} \int_0^r \rho r'^2 \,\mathrm{d}r',$$

R is radius of the sun, and m is the mass within a sphere of radius r.

The variational principle asserts that the eigenfrequencies are stationary with respect to variations in $\boldsymbol{\xi}_i$, i.e., if a perturbation in an eigenfunction is $\mathrm{O}(\varepsilon)$, then the perturbation in the eigenfrequency determined from Eq. (11) will be $\mathrm{O}(\varepsilon^2)$. Consequently, one can calculate small corrections to the frequencies due to changes in the physical conditions inside the Sun by linearizing Eq. (11) and using the unperturbed eigenfunctions.

From the variational principle one can obtain [3,36]:

$$\frac{\delta \omega_i^2}{\omega_i^2} = \int_0^R K_i^{(\rho,\gamma)} \frac{\delta \rho}{\rho} \,\mathrm{d}r + \int_0^R K_i^{(\gamma,\rho)} \frac{\delta \gamma}{\gamma} \,\mathrm{d}r, \tag{17}$$

where

$$K_i^{(\rho,\gamma)}(r) = \frac{\rho r^2}{E_i} \left\{ -\omega_i^2 [\xi_i^2 + l(l+1)\eta_i^2] + 2\xi_i (g_i' + 4\pi G \rho \xi_i - F_i g) + \frac{2l(l+1)}{r} \eta_i \Phi_i' - C_{1,i} g + 4\pi G (S_i - S_{1,i}) \right\}; \tag{18}$$

and

$$E_i = \omega_i^2 \int_0^R [\xi_i^2 + l(l+1)\eta_i^2] \rho r^2 \,\mathrm{d}r$$

is proportional to the energy of mode i;

$$F_i = \frac{1}{r}[2\xi_i - l(l+1)\eta_i], \qquad C_{1,i} = -\frac{1}{r^2} \int_0^r \gamma K_i' r'^2 \,\mathrm{d}r',$$

$$S_{1,i} = \int_r^R \rho C_{1,i} \,\mathrm{d}r', \qquad S_i = -2 \int_r^R \rho \xi_i F_i \,\mathrm{d}r', \tag{19}$$

$$K_i' = \left(\frac{\mathrm{d}\xi_i}{\mathrm{d}r} + F_i \right)^2 \equiv (\mathrm{div}\, \boldsymbol{\xi}_i)^2, \qquad K_i^{(\gamma,\rho)}(r) = \frac{r^2}{E_i} \gamma p K_i'.$$

If we define

$$\boldsymbol{z}_1 = \left(\frac{\delta\rho}{\rho}, \frac{\delta\gamma}{\gamma}\right), \qquad \boldsymbol{K}_i^{(1)} = (K_i^{(\rho,\gamma)}, K_i^{(\gamma,\rho)}), \tag{20}$$

then Eq. (17) can be written in the form

$$\frac{\delta\omega_i^2}{\omega_i^2} = \langle \boldsymbol{K}_i^{(1)} \cdot \boldsymbol{z}_1 \rangle, \tag{21}$$

where $\langle uv \rangle = \int_0^R uv \, \mathrm{d}r$.

Eqs. (17) or (21) provide integral constraints on unknown functions $\delta\rho/\rho$ and $\delta\gamma/\gamma$ with kernels $K_i^{(\rho,\gamma)}$ and $K_i^{(\gamma,\rho)}$. These kernels determine the sensitivity of the oscillation frequencies to density variations at constant adiabatic exponent γ and to variations of γ at constant ρ respectively. Integral equations similar to Eq. (17) can be obtained for some other parameters of solar structure. These equations are used for inferring the structure parameters from the relative differences between the observed frequencies and frequencies of a reference solar model. For a given reference model eigenfrequencies ω_i and kernels $K_i^{(\gamma,\rho)}$ and $K_i^{(\rho,\gamma)}$ can be computed numerically with standard methods.

2.2. Adjoint equations: kernel functions for structure properties

Integral equations (17) or (21) constitute the basis of the helioseismic inverse problem for inferring corrections to hydrostatic properties of a solar model (density, pressure, adiabatic exponent and their combinations) from the differences between the observed and model frequencies.

2.2.1. Kernel transformation: method of adjoint equations

The hydrostatic structure of the Sun is uniquely determined by the two 'primary' properties: density $\rho(r)$ and the adiabatic exponent $\gamma(r)$. Other, 'secondary' properties of the solar structure, such as the squared sound speed $c^2 = \gamma p/\rho$, the parameter of convective stability

$$A^* = \frac{1}{\gamma}\frac{\mathrm{d}\log p}{\mathrm{d}\log r} - \frac{\mathrm{d}\log\rho}{\mathrm{d}\log r},$$

temperature T or abundances of helium, Y, and heavier elements, Z, can be determined from ρ and γ using the equations of stellar structure. These equations describe the hydrostatic and thermal equilibria and the thermodynamic state of the solar plasma. Some of the 'secondary' properties (e.g. c^2 and A^*) can be determined using only the hydrostatic equations, while others (e.g. T and Y) require both the hydrostatic and thermodynamic equations. The latter involve some assumptions about microscopic properties of the solar plasma, which are not completely understood. These uncertainties may result in systematic errors in the inversion results. On the other hand, helioseismic data may provide some constraints on the microscopic properties (e.g. [21,23]).

In the helioseismic applications, it is often of interest to obtain direct estimates of these ('secondary') properties from the oscillation frequencies. Such a situation arises, for instance, when the available frequency information allows the determination of solar properties only in some particular regions of the solar interior. The integral equations which relates the variations of the 'secondary' properties to the frequency difference can be obtained by the method of adjoint functions [40,54].

The idea of this method is very simple. The relation between the 'primary', z_1, and 'secondary', z_2, properties that follows from the linearized stellar structure equations can be written in the following symbolic form:

$$\mathscr{A} z_1 = z_2, \tag{22}$$

where $\mathscr{A}$ is a linear operator. If $\boldsymbol{K}^{(2)}$ is the integral kernel for z_2 then according to Eq. (21) the relative frequency differences can be expressed in terms of both z_1 and z_2:

$$\delta\omega^2/\omega^2 = \langle \boldsymbol{K}^{(1)} z_1 \rangle = \langle \boldsymbol{K}^{(2)} z_2 \rangle. \tag{23}$$

Then using Eq. (22) and operator $\mathscr{A}^*$ adjoint to $\mathscr{A}$ we obtain

$$\langle \boldsymbol{K}^{(1)} z_1 \rangle = \langle \boldsymbol{K}^{(2)} z_2 \rangle = \langle \boldsymbol{K}_2, \mathscr{A} z_1 \rangle = \langle \mathscr{A}^* \boldsymbol{K}^{(2)}, z_1 \rangle. \tag{24}$$

Comparing the first and last terms of Eq. (24) we obtain the equation for the 'secondary' kernels, $\boldsymbol{K}^{(2)}$:

$$\mathscr{A}^* \boldsymbol{K}^{(2)} = \boldsymbol{K}^{(1)}, \tag{25}$$

which is adjoint to the structure equation (22).

Generally, the relation between the 'primary' and 'secondary' properties of the solar structure (Eq. (22)) is obtained from the equations of hydrostatic and thermal balance (see Section 2.2.2) and constitutes a system of linear differential and algebraic equations:

$$\frac{\mathrm{d}\boldsymbol{y}}{\mathrm{d}x} = A\boldsymbol{y} + Bz_2, \tag{26}$$

$$z_1 = C\boldsymbol{y} + Dz_2, \tag{27}$$

where $x = \log(r)$ and $\boldsymbol{y}(x)$ is a vector-function of some properties of the stellar structure different from z_1 and z_2 (e.g. gas pressure and fractional mass). Eqs. (26) and (27) are complemented by the boundary conditions of regularity at the stellar center and surface.

To find a kernel function $\boldsymbol{K}_i^{(2)}$ for z_2 we introduce a new vector-function $\boldsymbol{w}=(w_1, w_2)$ and consider the inner product of $\boldsymbol{w}$ with Eq. (25):

$$\left\langle \boldsymbol{w} \cdot \frac{\mathrm{d}\boldsymbol{y}}{\mathrm{d}x} \right\rangle = \langle \boldsymbol{w} \cdot A\boldsymbol{y} \rangle + \langle \boldsymbol{w} \cdot Bz_2 \rangle.$$

Using integration by parts and assuming that

$$\boldsymbol{w} \cdot \boldsymbol{y} = 0 \quad \text{at both} \quad r = 0 \quad \text{and} \quad r = R, \tag{28}$$

we find

$$-\left\langle \boldsymbol{y} \cdot \frac{\mathrm{d}\boldsymbol{w}}{\mathrm{d}x} \right\rangle = \langle \boldsymbol{y} \cdot A^{\mathrm{T}} \boldsymbol{w} \rangle + \langle \boldsymbol{w} \cdot Bz_2 \rangle, \tag{29}$$

where A^{T} is transposition of matrix A. Since kernels $\boldsymbol{K}^{(1)}$ and $\boldsymbol{K}^{(2)}$ satisfy Eq. (23), from Eq. (27) we have

$$\langle \boldsymbol{K}^{(1)} \cdot C\boldsymbol{y} \rangle + \langle \boldsymbol{K}^{(1)} \cdot Dz_2 \rangle = \langle \boldsymbol{K}^{(2)} \cdot z_2 \rangle. \tag{30}$$

If $\boldsymbol{w}$ is such that

$$\langle \boldsymbol{K}^{(1)} \cdot C\boldsymbol{y} \rangle = \langle \boldsymbol{w} \cdot Bz_2 \rangle,$$

then we obtain

$$-\left\langle \boldsymbol{y}\cdot\frac{\mathrm{d}\boldsymbol{w}}{\mathrm{d}x}\right\rangle = \langle \boldsymbol{y}\cdot A^{\mathrm{T}}\boldsymbol{w}\rangle + \langle \boldsymbol{w}\cdot B\boldsymbol{z}_2\rangle = \langle \boldsymbol{y}\cdot A^{\mathrm{T}}\boldsymbol{w}\rangle + \langle \boldsymbol{y}\cdot C^{\mathrm{T}}\boldsymbol{K}^{(1)}\rangle \tag{31}$$

and

$$\langle \boldsymbol{z}_2\cdot\boldsymbol{K}^{(2)}\rangle - \langle \boldsymbol{z}_2\cdot D^{\mathrm{T}}\boldsymbol{K}^{(1)}\rangle = \langle \boldsymbol{z}_2\cdot B^{\mathrm{T}}\boldsymbol{w}\rangle, \tag{32}$$

from Eqs. (29) and (30), respectively. Eqs. (31) and (32) will be valid for arbitrary structure variables $\boldsymbol{z}_2$ and $\boldsymbol{y}$, if

$$\frac{\mathrm{d}\boldsymbol{w}}{\mathrm{d}x} = -A^{\mathrm{T}}\boldsymbol{w} - C^{\mathrm{T}}\boldsymbol{K}^{(1)}, \tag{33}$$

$$\boldsymbol{K}^{(2)} = D^{\mathrm{T}}\boldsymbol{K}^{(1)} + B^{\mathrm{T}}\boldsymbol{w}. \tag{34}$$

These two relations together with the boundary conditions (28) determine kernels $\boldsymbol{K}^{(2)}$ for the 'secondary' structure variable $\boldsymbol{z}_2$. Therefore, to find the kernels $\boldsymbol{K}^{(2)}$, one has to solve the system of differential equations (33) with boundary conditions (28), and then to make use of Eq. (34).

2.2.2. Examples of the kernel transformation

2.2.2.1. Kernels for isothermal sound speed and helium abundance. As an example, we derive kernels $\boldsymbol{K}_2$ for function $\boldsymbol{z}_2 = (\delta \ln u, \delta Y)$, where $u \equiv p/\rho$, the ratio of the gas pressure to density, which is approximately proportional to the ratio of the temperature to the molecular weight, and Y is the abundance of helium. These 'secondary' properties are related to the 'primary' properties, ρ and γ, through the hydrostatic equations:

$$\frac{\mathrm{d}p}{\mathrm{d}r} = -\frac{Gm\rho}{r^2}, \qquad \frac{\mathrm{d}m}{\mathrm{d}r} = 4\pi\rho r^2, \tag{35}$$

and the equation of state

$$\gamma = \gamma(p,\rho,Y). \tag{36}$$

The corresponding linearized equations are

$$\frac{\mathrm{d}}{\mathrm{d}x}\left(\frac{\delta p}{p}\right) = -V\left(\frac{\delta m}{m} - \frac{\delta p}{p} + \frac{\delta\rho}{\rho}\right), \tag{37}$$

$$\frac{\mathrm{d}}{\mathrm{d}x}\left(\frac{\delta m}{m}\right) = U\left(-\frac{\delta m}{m} + \frac{\delta\rho}{\rho}\right), \tag{38}$$

$$\frac{\delta u}{u} = \frac{\delta p}{p} - \frac{\delta\rho}{\rho}, \tag{39}$$

$$\frac{\delta\gamma}{\gamma} = \left(\frac{\partial\ln\gamma}{\partial\ln p}\right)_{\rho,Y}\frac{\delta p}{p} + \left(\frac{\partial\ln\gamma}{\partial\ln\rho}\right)_{p,Y}\frac{\delta\rho}{\rho} + \left(\frac{\partial\ln\gamma}{\partial Y}\right)_{p,\rho}\delta Y, \tag{40}$$

where

$$x = \ln r, \quad V = -\frac{\mathrm{d}\ln p}{\mathrm{d}\ln r} = \frac{Gm\rho}{rp} \quad \text{and} \quad U = \frac{\mathrm{d}\ln m}{\mathrm{d}\ln r} = \frac{4\pi\rho r^3}{m}.$$

Boundary conditions for Eqs. (37) and (38) are the regularity conditions at $r = 0$, and $\delta m/m = 0$ at $r = R$.

Eqs. (37)–(40) (and similar equations for other 'secondary' variables) can be represented in the matrix form

$$\frac{\mathrm{d}\boldsymbol{y}}{\mathrm{d}x} = A_1\boldsymbol{y} + B_1\boldsymbol{z}_1 + B_2\boldsymbol{z}_2, \tag{41}$$

$$D_1\boldsymbol{z}_1 = C_1\boldsymbol{y} + D_2\boldsymbol{z}_2, \tag{42}$$

where $\boldsymbol{y} = (\delta p/p, \delta m/m)$, $\boldsymbol{z}_1 = (\delta\rho/\rho, \delta\gamma/\gamma)$, $\boldsymbol{z}_2 = (\delta u/u, \delta Y)$, A_1, B_1, B_2, C_1, D_1 and D_2 are (2×2)-matrices:

$$A_1 = \begin{pmatrix} V & -V \\ 0 & -U \end{pmatrix}, \quad B_1 = \begin{pmatrix} -V & 0 \\ U & 0 \end{pmatrix}, \quad B_2 = \begin{pmatrix} 0 & 0 \\ 0 & 0 \end{pmatrix}, \tag{43}$$

$$D_1 = \begin{pmatrix} 1 & 0 \\ -\left(\dfrac{\partial \ln\gamma}{\partial \ln\rho}\right)_{p,Y} & 1 \end{pmatrix}, \quad C_1 = \begin{pmatrix} 1 & 0 \\ \left(\dfrac{\partial \ln\gamma}{\partial \ln p}\right)_{\rho,Y} & 0 \end{pmatrix}, \tag{44}$$

$$D_2 = \begin{pmatrix} -1 & 0 \\ 0 & \left(\dfrac{\partial \ln\gamma}{\partial Y}\right)_{p,\rho} \end{pmatrix}. \tag{45}$$

Since $\det(D_1) \neq 0$ we can reduce Eqs. (41) and (42) to the standard form of Eqs. (26) and (27) introduced in the previous section:

$$\frac{\mathrm{d}\boldsymbol{y}}{\mathrm{d}x} = A\boldsymbol{y} + B\boldsymbol{z}_2, \tag{46}$$

$$\boldsymbol{z}_1 = C\boldsymbol{y} + D\boldsymbol{z}_2, \tag{47}$$

where

$$A = A_1 + B_1D_1^{-1}C_1, \quad B = B_1D_1^{-1}D_2 + B_2, \quad C = D_1^{-1}C_1, \quad D = D_1^{-1}D_2. \tag{48}$$

Using these matrices one can determine kernel functions $\boldsymbol{K}_2 = \left(K^{(u,Y)}, K^{(Y,u)}\right)$ by solving Eqs. (33) and (34).

2.2.2.2. Kernels for the parameter of convective stability. The parameter of convective stability

$$A^* = \frac{1}{\gamma}\frac{\mathrm{d}\log p}{\mathrm{d}\log r} - \frac{\mathrm{d}\log\rho}{\mathrm{d}\log r} \tag{49}$$

plays an important role for the internal structure of the Sun. When this parameter is positive the solar structure is stable against convection, and when it is negative the structure is unstable. In the bulk of the convection zone A^* is negative and close to zero, in the upper convection zone this parameter experiences a sharp minimum near the surface where highly unstable convective motions (granulation) are developed.

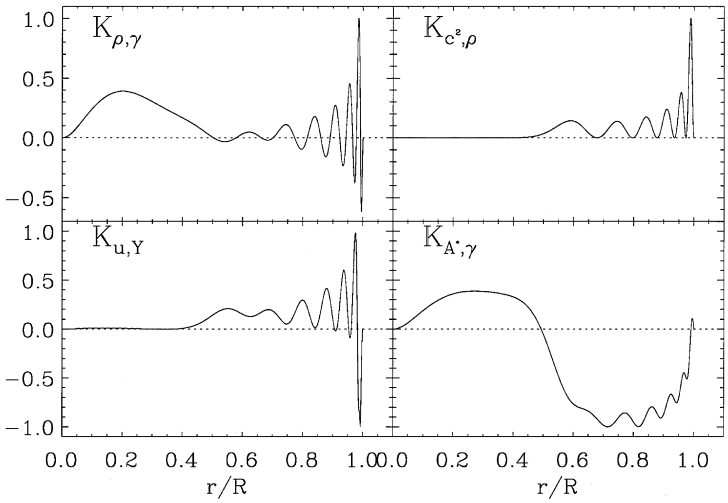

Fig. 2. Integral kernels for the acoustic mode with angular degree, $l = 10$, and radial order, $n = 6$. $K_{\rho,\gamma}$ is the kernel for density, ρ, at constant adiabatic exponent, γ; $K_{c^2,\rho}$ is the kernel for the squared sound speed, c^2, at constant ρ; $K_{u,Y}$ is the kernel for function u, – the ratio pressure, p, to density at constant helium abundance, Y; and $K_{A^*,\gamma}$ is the kernel for the parameter of convective stability, A^*, at constant γ.

In this case, we add to Eqs. (37) and (38) the linearized equation (49):

$$\frac{\mathrm{d}}{\mathrm{d}x}\left(\frac{\delta\rho}{\rho}\right) = V_g\left(\frac{\delta p}{p} - \frac{\delta m}{m} - \frac{\delta\rho}{\rho} + \frac{\delta\gamma}{\gamma}\right) - \delta A^*, \tag{50}$$

where $V_g = V/\gamma$. Defining $\boldsymbol{y} = (\delta p/p, \delta m/m, \delta\rho/\rho)$, $\boldsymbol{z}_1 = (\delta\rho/\rho, \delta\gamma/\gamma)$, $\boldsymbol{z}_2 = (\delta A^*, \delta\gamma/\gamma)$, we obtain Eqs. (46) and (47) with the following matrices:

$$A = \begin{pmatrix} V & -V & -V \\ 0 & -U & -U \\ V_g & -V_g & -V_g \end{pmatrix}, \quad B = \begin{pmatrix} 0 & 0 \\ 0 & 0 \\ -1 & V_g \end{pmatrix}, \quad C = \begin{pmatrix} 0 & 0 & 1 \\ 0 & 0 & 0 \end{pmatrix}, \quad D = \begin{pmatrix} 0 & 0 \\ 0 & 1 \end{pmatrix}. \tag{51}$$

Then, with these matrices the kernel function $\boldsymbol{K}^{(2)} = \left(K^{(A^*,\gamma)}, K^{(\gamma,A^*)}\right)$ is determined from Eqs. (33) and (34) [22].

Similar transformations of integral kernels can be derived for other appropriate pairs of unknown functions of solar structure [26,27,39,41]. It is important to note that the integral kernels for temperature and element abundances in the solar radiative core, which are important in astrophysical applications (e.g. the solar neutrino problem), can be determined by including the equations of thermal equilibrium in addition to the hydrostatic equations [26,27].

Examples of the kernel functions for different pairs of the solar structure variables are shown in Fig. 2.

2.3. Inversion methods

The variational principle and the method of adjoint functions described in the previous section allow us to determine linear integral relations between the observed quantities, relative frequency

differences between the Sun and a reference solar model, and the deviations of solar properties from this model. These relations constitute the linear inverse problem of determining the solar structure. This problem can be solved by standard regularization methods, such as the method of optimally localized averages [4] or the regularized least-squares method [77]. However, there are some specific features of this inverse problem such as two unknown functions in the integral constraints, and additional constraints to account for non-adiabatic effects which are not included in the variational principle. These problems are considered in this section.

2.3.1. Optimally localized averages

From a finite number of measured frequencies with errors, the unknown functions can be determined from Eq. (17) only with a finite spatial resolution; in other words, only certain average values of these functions can be determined.

We adopt a standard Backus–Gilbert inversion method [4,5] to compute the optimally localized averages of solar parameters. For instance, if $f(r)$ and $g(r)$ are two independent properties of the solar structure, which are related to the variations of eigenfrequencies via the integral relations

$$\frac{\delta\omega_i^2}{\omega_i^2} = \int_0^R K_i^{(f,g)} \frac{\delta f}{f}\,\mathrm{d}r + \int_0^R K_i^{(g,f)} \frac{\delta g}{g}\,\mathrm{d}r, \tag{52}$$

where $K_i^{(f,g)}$ and $K_i^{(g,f)}$ are the corresponding seismic kernels, then the localized averages of the variations of these properties at $r = r_0$ are determined as linear combinations of the frequency variations:

$$\left(\overline{\frac{\delta f}{f}}\right)_{r_0} = \sum_{i=1}^{N} a_i^{(f,g)}(r_0) \frac{\delta\omega_i^2}{\omega_i^2}, \tag{53}$$

$$\left(\overline{\frac{\delta g}{g}}\right)_{r_0} = \sum_{i=1}^{N} a_i^{(g,f)}(r_0) \frac{\delta\omega_i^2}{\omega_i^2}, \tag{54}$$

where $a_i^{(f,g)}(r_0)$ and $a_i^{(g,f)}(r_0)$ are coefficients for the optimal averaging kernels localized at $r = r_0$:

$$A^{(f,g)}(r_0, r) = \sum_{i=1}^{N} a_i^{(f,g)}(r_0) K_i^{(f,g)}(r), \tag{55}$$

$$A^{(g,f)}(r_0, r) = \sum_{i=1}^{N} a_i^{(g,f)}(r_0) K_i^{(g,f)}(r). \tag{56}$$

The coefficients of these linear combinations are obtained from a δ-ness criterion for the averaging kernels for one of the variables while minimizing the contribution of the other variable. If the δ-ness criterion provides the averaging kernels localized at $r = r_0$ then Eqs. (53) and (54) give estimates of $\delta f/f$ and $\delta g/g$ averaged around r_0.

For instance, for estimating $\delta f/f$, the δ-ness criterion for $A^{(f,g)}(r_0, r)$ is complemented by the minimization of the averaging function of the other variable, $\delta g/g$:

$$B^{(f,g)}(r_0, r) = \sum_{i=1}^{N} a_i^{(f,g)}(r_0) K_i^{(g,f)}(r).$$

In this case, coefficients $a_i^{(f,g)}$ are determined by minimizing the following quadratic function:

$$M(r_0,A,\alpha,\beta)=\int_0^R J(r_0,r)[A^{(f,g)}(r_0,r)]^2\,\mathrm{d}r+\beta\int_0^R [B^{(f,g)}(r_0,r)]^2\,\mathrm{d}r+\alpha\sum_{i,j}E_{ij}a_i^{(f,g)}a_j^{(f,g)}, \quad (57)$$

where $J(r_0,r)=12(r-r_0)^2$, E_{ij} is a covariance matrix of observational errors, and α and β are the regularization parameters. The first integral in Eq. (57) represents the Backus–Gilbert criterion of δ-ness for $A^{(f,g)}(r_0,r)$; the second term minimizes the contribution from $B^{(f,g)}(r_0,r)$, thus, effectively eliminating the second unknown function, $\delta g/g$; and the last term minimizes the errors.

The numerical procedure to compute $a_i^{(f,g)}(r_0)$ for given α and β is to substitute Eqs. (55) and (56) into Eq. (57), and, then, minimize M as a positively defined quadratic function of $a_i^{(f,g)}$ subject to the normalization constraint:

$$\int_0^R A^{(f,g)}(r_0,r)\,\mathrm{d}r\equiv\sum_{i=1}^N a_i^{(f,g)}(r_0)\int_0^R K^{(f,g)}(r_0,r)\,\mathrm{d}r=1. \quad (58)$$

If we define

$$v_i=\int_0^R K_i^{(f,g)}(r)\,\mathrm{d}r,\quad S_{p,ij}^{(f,g)}=12\int_0^R r^p K_i^{(f,g)}(r)K_j^{(f,g)}(r)\,\mathrm{d}r, \quad (59)$$

$$S_{ij}^{(f,g)}=r_0^2S_{0,ij}^{(f,g)}-2r_0S_{1,ij}^{(f,g)}+S_{2,ij}^{(f,g)},\quad S_{ij}^{(g,f)}=12\int_0^R K_i^{(g,f)}(r)K_j^{(g,f)}(r)\,\mathrm{d}r$$

and

$$W_{ij}=S_{ij}^{(f,g)}+\beta S_{ij}^{(g,f)}+\alpha E_{ij},$$

where $i,j=1,\ldots,N$, then coefficients $a_i^{(f,g)}(r_0)$ satisfy

$$W\boldsymbol{a}+\lambda\boldsymbol{v}=0 \quad (60)$$

and

$$\boldsymbol{v}\cdot\boldsymbol{a}=1, \quad (61)$$

where $\boldsymbol{a}=(a_1^{(f,g)},\ldots,a_N^{(f,g)})$, $\boldsymbol{v}=(v_1,\ldots,v_N)$, and λ is a Lagrange multiplier. From Eqs. (60) and (61) we obtain

$$\boldsymbol{a}=\frac{\boldsymbol{y}}{(\boldsymbol{y}\cdot W\boldsymbol{y})}, \quad (62)$$

where

$$\boldsymbol{y}=W^{-1}\boldsymbol{v}. \quad (63)$$

Then, the localized averages of $\delta f/f$ are estimated from

$$\left(\overline{\frac{\delta f}{f}}\right)_{r_0}=\sum_{i=1}^N a_i^{(f,g)}(r_0)\frac{\delta\omega_i^2}{\omega_i^2}=\int_0^R A^{(f,g)}(r_0,r)\frac{\delta f}{f}\,\mathrm{d}r+\left(\overline{\frac{\delta g}{g}}\right), \quad (64)$$

where

$$\left(\overline{\frac{\delta g}{g}}\right)=\int_0^R B^{(f,g)}(r_0,r)\frac{\delta g}{g}\,\mathrm{d}r \quad (65)$$

is the contribution of the second, 'eliminated', variable. This contribution causes errors in the estimated localized averages of the first function, and, therefore, has to be made sufficiently small, e.g.

$$\left(\frac{\overline{\delta g}}{g}\right)_{\max} \leqslant \varepsilon, \tag{66}$$

where $\varepsilon = \left(\sum_{i,j} a_i^{(f,g)} a_j^{(f,g)} E_{ij}\right)^{1/2}$ is an estimate of random errors in the inversion results. If we assume that $|\delta g/g| < C$, then, from Eqs. (65) and (66) we obtain the following criterion for choosing the regularization parameter β:

$$\int_0^R B^{(f,g)}(r_0, r)\,\mathrm{d}r \leqslant C^{-1}\varepsilon. \tag{67}$$

The regularization parameter α is determined as a trade-off between the spatial resolution and error magnification [5]. The resolution of inversions is characterized by the spread of the averaging kernels

$$s_0 = \sum_{i,j} a_i^{(f,g)} a_j^{(f,g)} S_{ij}^{(f,g)} \tag{68}$$

and their width

$$w = \sum_{i,j} a_i^{(f,g)} a_j^{(f,g)} S_{2,ij}^{(f,g)} - \frac{[\sum_{i,j} a_i^{(f,g)} a_j^{(f,g)} S_{1,ij}^{(f,g)}]^2}{\sum_{i,j} a_i^{(f,g)} a_j^{(f,g)} S_{0,ij}^{(f,g)}}. \tag{69}$$

The central location of the averaging kernels can be estimated from

$$c(r_0) = \frac{\sum_{i,j} a_i^{(f,g)}(r_0) a_j^{(f,g)}(r_0) S_{1,ij}^{(f,g)}}{\sum_{i,j} a_i^{(f,g)}(r_0) a_j^{(f,g)}(r_0) S_{0,ij}^{(f,g)}}. \tag{70}$$

2.3.2. Nonadiabatic effects

Nonadiabatic effects near the solar surface cause systematic frequency shifts which may affect the inversion results. If the observed frequencies are

$$\omega_{\mathrm{obs},i} = \omega_{\mathrm{ad},i} + \delta\omega_{\mathrm{nonad},i},$$

then the localized averages of $\delta f/f$ are

$$\left(\frac{\overline{\delta f}}{f}\right)_{\mathrm{obs}} = \left(\frac{\overline{\delta f}}{f}\right)_{\mathrm{ad}} + \sum_{i=1}^{N} a_i^{(f,g)} \frac{\delta\omega_{\mathrm{nonad},i}^2}{\omega_i^2}, \tag{71}$$

where $\omega_i \equiv \omega_{\mathrm{ad},i}$.

Therefore, the nonadiabatic effects cause systematic errors in the localized averages estimated by using the adiabatic variational principle. In the Sun, most non-adiabatic effects occur near the solar surface. In this case, as suggested in [14,20], the nonadiabatic frequency shift can be approximated by a smooth function of frequency, $F(\omega)$ scaled with the factor, $Q \equiv I(\omega)/I_0(\omega)$, where $I(\omega)$ is the mode inertia (Eq. (16)), and $I_0(\omega)$ is the mode inertia of radial modes ($l = 0$), calculated at frequency ω, that is

$$\frac{\delta\omega_{\mathrm{nonad},i}^2}{\omega_i^2} = F(\omega_i)/Q(\omega_i). \tag{72}$$

If the function $F(\omega)$ can be approximated by a polynomial function of degree K:

$$F(\omega_i) = \sum_{k=0}^{K} c_k \omega_i^k, \tag{73}$$

then the influence of the nonadiabatic effects can be reduced by applying $K+1$ additional constraints for a_i:

$$\sum_{i=1}^{N} a_i \omega_i^k Q(\omega_i) = 0, \quad k = 0, \ldots, K. \tag{74}$$

These constraints are considered together with the Eq. (58) in the minimization procedure of the quadratic function (57). If we represent constraints (58) and (74) in the matrix form

$$B\boldsymbol{a} = \boldsymbol{c}, \tag{75}$$

then the minimization procedure leads to the equation

$$W\boldsymbol{a} + \boldsymbol{\lambda} B = 0, \tag{76}$$

where $\boldsymbol{\lambda} = (\lambda_1, \ldots, \lambda_{K+2})$ are Lagrange multipliers. Finally, from Eqs. (75) and (76) we obtain the coefficients of the optimally localized averages:

$$\boldsymbol{a} = \left(W^{-1}B^{\mathrm{T}}\right)\left(BW^{-1}B^{\mathrm{T}}\right)^{-1}\boldsymbol{c}, \tag{77}$$

where B^{T} is a matrix transposed to B.

The function $F(\omega)$ can be also represented in terms of Legendre polynomials [20]

$$F(\omega) = \sum_k c_k P_k\left(\frac{2\omega - \omega_{\max} - \omega_{\min}}{\omega_{\max} - \omega_{\min}}\right), \tag{78}$$

where $\omega_{\min}$ and $\omega_{\max}$ are the boundaries of the observed frequency range.

2.3.3. Regularized least-squares techniques

The regularized least-squares (RLS) method [77] is based on minimization of the quantity

$$\mathscr{E} \equiv \sum_i \frac{1}{\sigma_i^2}\left[\frac{\delta\omega_i^2}{\omega_i^2} - \int_0^R \left(K_i^{(f,g)}\frac{\delta f}{f} + K_i^{(g,f)}\frac{\delta g}{g}\right) \mathrm{d}r - \frac{F(\omega_i)}{Q}\right]^2 + \int_0^R \left[\alpha_1\left(L_1\frac{\delta f}{f}\right)^2 + \alpha_2\left(L_2\frac{\delta g}{g}\right)^2\right] \mathrm{d}r, \tag{79}$$

in which the unknown structure correction functions, $\delta f/f$ and $\delta g/g$, are both represented by piece-wise linear functions or by cubic splines, and the coefficients in these expansions are determined together with coefficients c_k in the presentation of F (Eqs. (73) or (78)). The second integral specifies smoothness constraints for the unknown functions, in which L_1 and L_2 are linear differential operators, e.g. $L_{1,2} = \mathrm{d}^2/\mathrm{d}^2 r$; σ_i are error estimates of the relative frequency differences.

In this inversion method, the estimates of the structure corrections are, once again, linear combinations of the frequency differences obtained from observations, and corresponding averaging kernels exist too [75]. However, unlike the OLA kernels $A(r_0; r)$, the RLS averaging kernels may have negative side-lobes and significant peaks near the surface, thus making interpretation of the inversion results to some extent ambiguous. This technique has been used in [2,20,44].

If the variations of the structure properties are represented in a parametric form then the unknown parameters can be evaluated from the helioseismic equations (52) by using a least-squares technique. Kosovichev [41] has applied this parametric inversion technique for determining the depth of the convection zone and the helium abundance. Finally, 'super-resolution' techniques can be developed by applying, for instance, nonlinear constraints in order to study some particular features of the interior structure, like overshooting and other sharp variations of the interior properties [43]. In addition to the inversions, model calibrations are used to estimate the parameters of the solar structure (e.g. [7,11,57]).

2.4. Results

As an example, I present the results of inversion of the recent data obtained from the SOI-MDI instrument on board the SOHO space observatory. The data represent 2176 frequencies of solar oscillations of the angular degree, l, from 0 to 250. These frequencies were obtained by fitting peaks in the oscillation power spectra from a 360-day observing run, between May 1, 1996 and April 25, 1997.

Two different methods have been used to estimate the frequencies of the solar normal modes from the oscillation power spectra [63]. In the first, so-called 'mean-multiplet' method [67], the power spectral peaks are assumed to have a symmetric Lorentzian shape, and a maximum likelihood method is employed to determine the parameters of Lorentzian profiles. The peaks are fit simultaneously in all of the $2l+1$ individual power spectra for each rotationally split multiplet so that the effects of overlapping peaks can be included in the fits. These $2l+1$ frequencies are effectively averaged to yield a single mean frequency, ω_{nl}, for that multiplet. The second frequency estimation technique employs the m-averaged power spectra rather than the $2l+1$ individual power spectra.

The reference solar model chosen for this inversion is described in [12]. This model used the OPAL equation of state and opacities [64,65]. Nuclear reaction parameters were obtained from [6]. Helium and heavy-element settling was included, using the Michaud and Proffitt coefficients [62]. The present value of the ratio of the heavy element abundance to the hydrogen abundance on the solar surface is 0.0245, while the age of the present Sun was assumed to be 4.6 Gyr.

Fig. 3 shows the frequency difference scaled with the factor Q (cf. Eq. (72)) which varies between 0.28 and 1. This difference depends mainly on frequency alone meaning that most of the difference

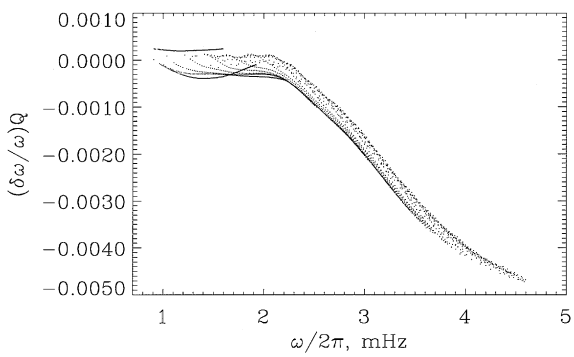

Fig. 3. The scaled relative frequency difference between the Sun and the standard solar model.

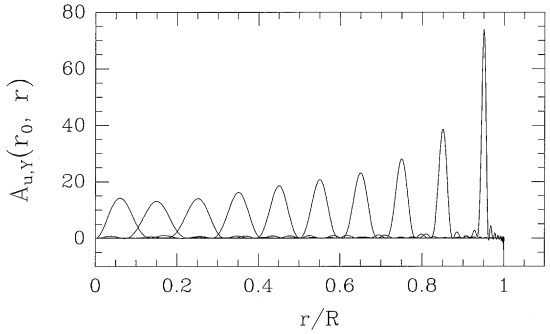

Fig. 4. A sample of the optimally localized averaging kernels for the structure function, u, the ratio of pressure, p, to density, ρ.

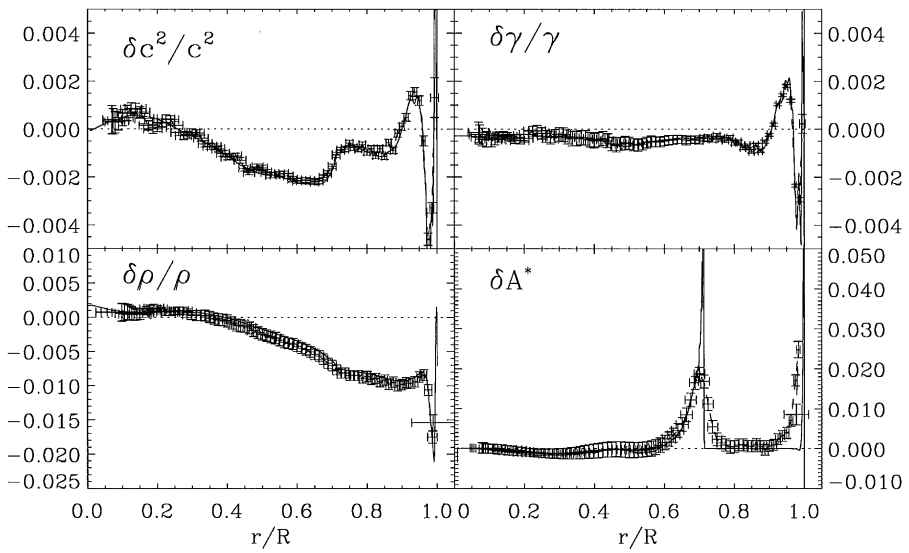

Fig. 5. The results of test inversions (points with the error bars, connected with dashed curves) of frequency differencies between two solar models for the squared sound speed, c^2, the adiabatic exponent, γ, the density, ρ, and the parameter of convective stability, A^*. The solid curves show the actual differences between the two models. Random Gaussian noise was added to the frequencies of a test solar model. The vertical bars show the formal error estimates, the horizontal bars show the characteristic width of the localized averaging kernels. The central points of the averages are plotted at the centers of gravity of the averaging kernels.

between the Sun and the reference solar model is in the near-surface layers. However, there is also a significant scatter along the general frequency trend. This scatter is due to the variations of the structure in the deep interior, and it is the basic task of the inversion methods to uncover the variations.

The inversion method applied to these data was the optimally localized averaging described in Section 2.3.1. A sample of the localized averaging kernels is shown in Fig. 4. Fig. 5 shows the results of test inversions, in which frequencies of a solar model were used instead of the observed

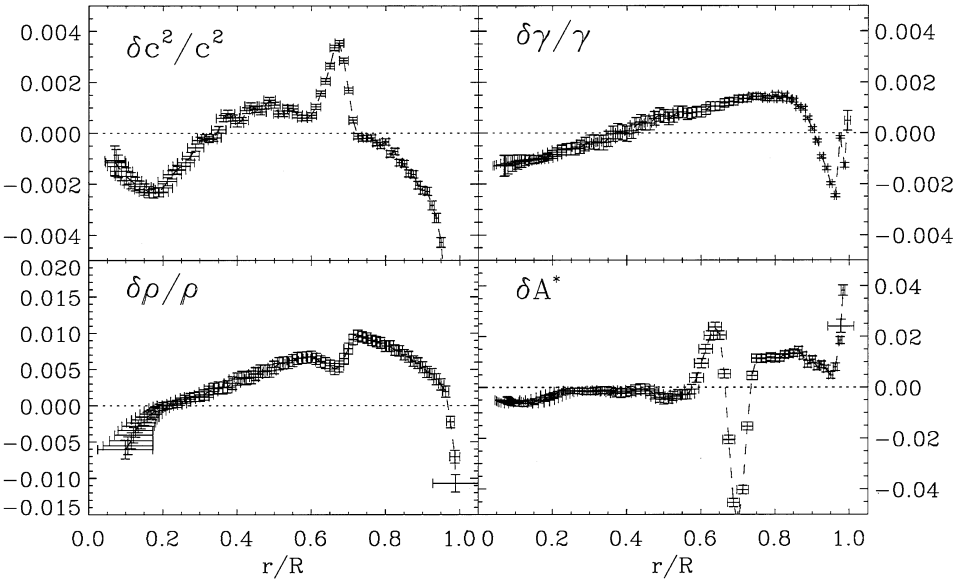

Fig. 6. The relative differences between the Sun and the standard solar model in the squared sound speed, c^2, the adiabatic exponent, γ, the density, ρ, and the parameter of convective stability, A^*, inferred from the solar frequencies determined from the 360-day series of SOHO MDI data.

frequencies. This test model was computed with the equation of state [55] instead of the OPAL equation of state employed in the reference model; the other input physics was the same. The theoretical frequencies of this model were perturbed with the Gaussian noise corresponding to the observational errors. The results of this inversion (Fig. 5) show good agreement between the inversion results and the actual differences. However, the sharp variations, like a peak in δA^* at the base of the convection zone, are smoothed. Also, the inner 5% of the Sun and the subsurface layers (outer 2–3%) are not resolved.

The inversion results for the 360-day SOI-MDI data are shown in Fig. 6. These results show that the differences between the inferred structure and the reference solar model are quite small, generally less than 1%. The small differences provide a justification for the linearization procedure of Section 2, based on the variational principle. This also means that the modern standard model of the Sun provides an accurate description of the solar properties. However, the inversions reveal significant deviations from the standard model, which lead to better understanding of the structure and evolution of the star, and have important applications in other fields of astrophysics [29,48]. For instance, the prominent peak of the squared sound speed, $\delta c^2/c^2$, at the base of the convection zone, $r/R \approx 0.7$, indicates on additional mixing which may be caused by rotational shear flows or by convective overshoot. The variation in the sound speed in the energy-generating core, $r/R < 0.2$, also provides evidence for a partial mixing [27].

The monotonic decrease of the adiabatic exponent, γ, in the core was recently explained by the relativistic corrections to the equation of state [23]. Near-surface variations of γ, in the zones of ionization of helium and hydrogen, and below these zones, are most likely caused by deficiencies in the theoretical models of the weakly coupled plasma in both OPAL and MHD equations of state.

The monotonic decrease of the squared sound speed variation in the convection zone ($r/R > 0.7$) is partly due to an error in the solar radius used to calibrate the standard model [71].

3. Inversions for solar rotation

3.1. Theory of rotational frequency splitting

The eigenfrequencies of a spherically symmetrical static star are degenerate with respect to the azimuthal number m. Rotation breaks the symmetry and splits each mode of radial order, n, and angular degree, l, into $(2l+1)$ components of $m=-l,\dots,l$ ('mode multiplets'). The rotational frequency splitting can be computed using a more general variational principle derived by Linden-Bell and Ostriker [53]. From this variational principle, one can obtain mode frequencies ω_{nlm} relative to the degenerate frequency ω_{nl} of the nonrotating star:

$$\Delta\omega_{nlm} \equiv \omega_{nlm} - \omega_{nl} = \frac{1}{I_{nl}} \int_V [m\boldsymbol{\xi}\cdot\boldsymbol{\xi}^* + \mathrm{i}\boldsymbol{e}_\Omega(\boldsymbol{\xi}\times\boldsymbol{\xi}^*)]\Omega\rho\,\mathrm{d}V, \tag{80}$$

where $\boldsymbol{e}_\Omega$ is the unit vector defining the rotation axis, and $\Omega=\Omega(r,\theta)$ is the angular velocity which is a function of radius r and co-latitude θ, and I_{nl} is the mode inertia (Eq. (16)).

Using Eq. (14) for the eigenfunctions, $\boldsymbol{\xi}$, Eq. (80) can be rewritten as a two-dimensional integral equation for $\Omega(r,\theta)$:

$$\Delta\omega_{nlm} = \int_0^R \int_0^\pi K^{(\Omega)}_{nlm}(r,\theta)\Omega(r,\theta)\,\mathrm{d}\theta\,\mathrm{d}r \tag{81}$$

where $K^{(\Omega)}_{nlm}(r,\theta)$, the rotational splitting kernels:

$$K^{(\Omega)}_{nlm}(r,\theta) = \frac{m}{I_{nl}} 4\pi\rho r^2 \left\{ (\xi^2_{nl} - 2\xi_{nl}\eta_{nl})(P^m_l)^2 + \eta^2_{nl}\left[\left(\frac{\mathrm{d}P^m_l}{\mathrm{d}\theta}\right)^2 - 2P^m_l\frac{\mathrm{d}P^m_l}{\mathrm{d}\theta}\frac{\cos\theta}{\sin\theta} + \frac{m^2}{\sin^2\theta}(P^m_l)^2\right]\right\}\sin\vartheta. \tag{82}$$

Here ξ_{nl} and η_{nl} are the radial components of eigenfunctions (14) of the mean spherically symmetric structure of the Sun, $P^m_l(\theta)$ is an associated normalized Legendre function ($\int_0^\pi (P^m_l)^2 \sin\theta\,\mathrm{d}\theta = 1$). The kernels are symmetric relative to the equator, $\theta=\pi/2$. Therefore, the frequency splittings are sensitive only to the symmetric component of rotation in the first approximation. The non-symmetric component can, in principle, be determined from the second-order correction to the frequency splitting [28], or from local helioseismic techniques, such as time-distance seismology and ring-diagram analysis [24,69].

For a given set of observed frequency splittings, $\Delta\omega_{nlm}$, Eq. (81) constitutes a two-dimensional linear inverse problem for the angular velocity, $\Omega(r,\theta)$. Details of the method for estimating the frequency splittings were given in [67]; see also [33] for another discussion of the data analysis issues. In order to increase the stability of the estimates, the $2l+1$ frequencies ω_{nlm} of individual modes within a given (n,l) multiplet can be parameterized in terms of a set of orthogonal polynomials

$\mathscr{P}_j^{(l)}(m)$ of degree j:

$$\omega_{nlm} = \omega_{nl} + 2\pi \sum_{j=1}^{j_{\max}} a_j(n,l)\mathscr{P}_j^{(l)}(m) \tag{83}$$

with generally fewer than $2l+1$ parameters a_j. The polynomials $\mathscr{P}_j^{(l)}(m)$ used in this expansion are defined by

$$\mathscr{P}_j^{(l)}(l) = l \quad \text{and} \quad \sum_{m=-l}^{l} \mathscr{P}_i^{(l)}(m)\mathscr{P}_j^{(l)}(m) = 0 \quad \text{for } i \neq j. \tag{84}$$

The polynomials are related to Clebsch–Gordan coefficients C_{lmj0}^{lm} by (e.g. [48])

$$\mathscr{P}_j^{(l)}(m) = \frac{l\sqrt{(2l-j)!(2l+j+1)!}}{(2l)!\sqrt{2l+1}} C_{lmj0}^{lm}. \tag{85}$$

From the symmetry properties of the splittings it follows that rotation contributes only to the a_j for odd j. The even a_j coefficients are related to the large-scale asphericity of the Sun, and their analysis is generally similar (e.g. [25]).

The expansion of the splittings in polynomials in m, as in Eq. (83), corresponds to an expansion of Ω as

$$\Omega(r,\theta) = \sum_{s=0}^{s_{\max}} \Omega_s(r) \frac{\mathrm{d}P_{2s+1}}{\mathrm{d}z}, \tag{86}$$

where $P_k(z)$ is a Legendre polynomial of $z = \cos\theta$ (e.g. [9,38]). The a coefficients and expansion functions for Ω are related by

$$2\pi a_{2j+1}(n,l) = \int_0^R K_{nlj}^{(a)}(r)\Omega_j(r)\,\mathrm{d}r, \tag{87}$$

for suitable kernels $K_{nlj}^{(a)}$ [59]. Thus, the original 2-D inverse problem can be decomposed into a series of independent 1-D inversions in r; this forms the basis for the so-called 1.5-D inversion methods.

3.2. Inversion methods

Inversion methods for inferring the 2-D rotation rate are substantially less developed and less robust than the methods of 1-D structure inversions discussed in Section 2, because the rotation inversion involves large data sets with 10^5–10^6 data points, and because these data are much less accurate than the mean multiplet frequencies used in the structure inversions. In this section, we discuss an asymptotic method which effectively averages the data according to the distribution of the lower turning points of acoustic modes. Also, modifications to the optimally localized averaging method which in its original formulation (Section 2) becomes impractical for the large data sets, are also discussed.

3.2.1. Asymptotic method

If the internal structure and rotation of the Sun vary smoothly, so that the parameter, $\varepsilon = (k_r r_0)^{-1}$, representing the ratio of the wavelength, $\lambda \simeq k_r^{-1}$ to the characteristic scale, r_0, of the solar properties

is small, one can apply an asymptotic (JWKB) approximation to Eqs. (5)–(8) or (10). This approximation is useful for inferring the internal structure and rotation because it substantially simplifies the inverse problem, provides a simple physical interpretation of the data and inversion results, and is sufficiently accurate in many cases. For the solar acoustic (p) modes, the wave number, k_r, is related to the oscillation frequency by the dispersion relation (e.g. [78])

$$k_r^2 = \frac{1}{\omega^2 c^2}(\omega^2 - L_l^2)(\omega^2 - N^2), \tag{88}$$

where c is the sound speed, $L_l^2 \equiv l(l+1)c^2/r^2$ is the Lamb frequency, $N^2 = gA^*/r$ is the Brunt–Väisälä frequency, and A^* is the parameter of convective stability (49). The squared wave number k_r^2 is positive in the region of wave propagation, and vanishes at the turning points, r_1 and r_2, specified by the conditions $\omega^2 = L_l^2$ and $\omega^2 = N^2$, respectively, which are points of total internal reflection of acoustic waves. These points define the lower (r_1) and upper (r_2) boundaries of the acoustic cavity. Since $\omega^2 \gg N^2$ for the solar acoustic oscillations everywhere except very close to the surface we can neglect the last term of Eq. (88) and assume that $r_2 \approx R$, where R is the solar radius.

We may seek a solution to the oscillation equations (10) in the form $\boldsymbol{\xi} \propto \exp(\mathrm{i}S(r))$, where $S(r)$ is written as a series in powers of ε. Retaining only the first-order term, one finds the following asymptotic solution to the radial eigenfunctions:

$$\xi_{nl} \simeq \frac{[\omega^2 - l(l+1)c^2/r^2]^{1/2}}{\omega\rho^{1/2}cr}\frac{1}{k_r^{1/2}}\sin\left(\int_r^{r_2} k_r\,\mathrm{d}r' - \frac{\pi}{4}\right), \tag{89}$$

$$\eta_{nl} \simeq \frac{[\omega^2 - N^2]^{1/2}}{\omega^2\rho^{1/2}r^2}\frac{1}{k_r^{1/2}}\cos\left(\int_r^{r_2} k_r\,\mathrm{d}r' - \frac{\pi}{4}\right). \tag{90}$$

These equations are valid in the wave propagation regions, far from the turning points.

In a similar way, we can derive an asymptotic approximation for the associate Legendre functions $P_l^m(z)$ where $z = \cos\theta$. For oscillations with $l \gg 1$, the functions $P_l^m(z)$ may be expanded in powers of $1/l$ (e.g. [56]):

$$P_l^m(z) = \left(\frac{2l+1}{\pi k_z(1-z^2)}\right)^{1/2}\cos\left(\int_{z_1}^{z} k_z\,\mathrm{d}z' - \frac{\pi}{4}\right), \tag{91}$$

where

$$\begin{aligned} k_z &= \frac{1}{(1-z^2)^{1/2}}\left[\left(l+\frac{1}{2}\right)^2 - \frac{m^2}{1-z^2}\right]^{1/2}, \\ z_{1,2} &= \mp\left[1 - \frac{m^2}{(l+1/2)^2}\right]^{1/2}, \quad z_1 < z < z_2, \end{aligned} \tag{92}$$

and z_1 and z_2, are turning points with respect to the angular coordinate.

Substituting the asymptotic eigenfunctions (Eqs. (89)–(91)) into Eqs. (81)–(82) and intergrating over rapidly varying trigonometric functions we arrive at an integral equation for the angular velocity Ω [47]:

$$\Delta\omega_{nlm} = \frac{m}{\pi I_{nl}}\int_x^{y_S}\int_{-\sqrt{\eta}}^{\sqrt{\eta}} \Omega(y,z)y\frac{\mathrm{d}\ln r}{\mathrm{d}y}(y-x)^{-1/2}(\eta - z^2)^{-1/2}\,\mathrm{d}z\,\mathrm{d}y, \tag{93}$$

where the asymptotic mode inertia is given by

$$I_{nl} = \int_x^{y_S} (y-x)^{-1/2} y \frac{\mathrm{d}\ln r}{\mathrm{d}y} \mathrm{d}y, \tag{94}$$

$x = (l+1/2)^2/\omega^2$, $y = r^2/c^2$, $\eta = 1 - m^2/(l+1/2)^2$, and y_S is the value of y at the solar surface, $r = R$.

Eq. (93) can be rewritten in the form of the two-dimensional Abel integral equation

$$\int_x^{y_S} \int_0^{\eta} \frac{\phi(y,t)\,\mathrm{d}t\,\mathrm{d}y}{(y-x)^{1/2}(\eta-t)^{1/2}} = G(x,\eta), \tag{95}$$

where

$$\phi(y,t) = \Omega(y,t) y t^{-1/2} \frac{\mathrm{d}\ln r}{\mathrm{d}y}, \quad G(x,\eta) = \pi \frac{\Delta\omega_{nlm}}{m} I_{nl}. \tag{96}$$

This equation can be solved in several ways. One approach is to apply Abel inversion to each of the inner integrals, as a result we obtain [47]

$$\phi(x,\eta) = \frac{1}{\pi^2} \frac{\partial^2}{\partial x \partial \eta} \int_0^{\eta} \int_x^{y_S} \frac{G(\mu,\nu)\,\mathrm{d}\mu\,\mathrm{d}\nu}{(\eta-\nu)^{1/2}(\mu-x)^{1/2}}. \tag{97}$$

Thus, in the case $l \gg 1$, where the asymptotic representation is valid, the inverse for the solar internal rotation can be solved by quadratures. The observed frequency splittings, $\Delta\omega_{nlm}/m$, are approximated by a two-dimensional function of the asymptotic variables $(l+1/2)/\omega$ and $(l+1/2)/m$. One should keep, in mind, however, that due to observational error regularization algorithms are required to keep the Abel inversion stable.

3.2.2. Optimally localized averaging methods

Similar to the 1-D case (Section 2.3.1) these methods explicitly form linear combinations of the data and corresponding kernels such that the resulting averaging kernels are, to the extent possible, localized near the target positions, r_0, θ_0, through appropriate choice of the coefficients $a_i^{(\Omega)}(r_0,\theta_0)$ (see [4]):

$$\bar{\Omega}(r_0,\theta_0) = \sum_{i=1}^{M} a_i^{(\Omega)}(r_0,\theta_0) d_i = \int_0^R \int_0^{\pi} \mathscr{K}(r_0,\theta_0,r,\theta)\Omega(r,\theta)\,\mathrm{d}\theta\,\mathrm{d}r, \tag{98}$$

where d_i is the observed property, frequency splitting $\Delta\omega_{nlm}$, or splitting coefficients $a_j(n,l)$ (83), $\mathscr{K}(r_0,\theta_0,r,\theta)$ is the averaging kernel given by

$$\mathscr{K}(r_0,\theta_0,r,\theta) = \sum_{i=1}^{M} a_i^{(\Omega)}(r_0,\theta_0) K_i^{(\Omega)}(r,\theta), \tag{99}$$

and M is the total number of data points. However, the application of the Backus–Gilbert [4] δ-ness criterion leads to $M \times M$ linear equations at each of the target positions. A modification suggested in [51,52,60] allows to keep the same matrix for all target points, and, thus, is computationally more efficient. In this formulation, sometimes called 'subtractive optimally localized averaging' (2dSOLA), the goal is to approximate $\mathscr{K}$ to a prescribed target $\mathscr{T}(r_0,\theta_0,r,\theta)$, by minimizing

$$\int_0^R \int_0^{\pi} [\mathscr{T}(r_0,\theta_0,r,\theta) - \mathscr{K}(r_0,\theta_0,r,\theta)]^2\,\mathrm{d}\theta\,\mathrm{d}r + \lambda \sum_{i=1}^{M} [\sigma_i a_i^{(\Omega)}(r_0,\theta_0)]^2 \tag{100}$$

subject to $\mathscr{K}$ being unimodular. Here the first term ensures that the averaging kernel is close to the target form, while the second controls the error in the inferred solution, the trade-off between the two being controlled by the parameter λ.

The results of this method depend on the choice of the target function, $\mathscr{T}(r_0, \theta_0, r, \theta)$, and, currently, there is no general recipe for choosing this function. One of the approaches is to employ Gaussian targets symmetrized around the equator, with the radial width chosen proportional to the local sound speed (e.g. [76]) and constant width in latitude. However, the Gaussian target kernels may lead to substantial side-lobes in the averaging kernels and confusing results near the boundaries because the seismic kernels vanish at the boundaries [50]. Larsen et al. [50] suggested modifying the target functions according to the behavior of the seismic kernels near the boundaries.

A simple implementation of the above method would require the factorization of one or more $M \times M$ matrices, and hence would be prohibitively expensive computationally for two-dimensional inversion, because M may be so large, 10^5–10^6. Efficient algorithms have been developed by exploiting the special structure of the integral kernels $K^{(\Omega)}_{nlm}(r, \theta)$. Eq. (82) can be rewritten in the form

$$K^{(\Omega)}_{nlm}(r, \theta) = F_{nl}(r) G_{lm}(\theta) + H_{nl}(r) J_{lm}(\theta), \tag{101}$$

where $F_{nl}(r) = 4\pi\rho r^2(\xi^2_{nl} - 2\xi_{nl}\eta_{nl})/I_{nl}$, $H_{nl}(r) = 4\pi\rho r^2 \eta^2_{nl}/I_{nl}$, $G_{lm}(\theta) = m \sin\theta (P^m_l)^2$, and

$$J_{lm}(\theta) = m \sin\theta \left[\left(\frac{\mathrm{d}P^m_l}{\mathrm{d}\theta} \right)^2 - 2P^m_l \frac{\mathrm{d}P^m_l}{\mathrm{d}\theta} \frac{\cos\theta}{\sin\theta} + \frac{m^2}{\sin^2\theta} (P^m_l)^2 \right].$$

For the SOI-MDI data, for instance, $l \in [1, 250], n \in [0, 25]$, and $m \in [-l, l]$, and, thus, $M \approx 1.5 \cdot 10^6$. However, the index n appears only in the radial functions, F and G, and does not appear in the angular functions, G and J. Moreover, the second term is usually much smaller than the first term in Eq. (101). These properties can be used for developing efficient numerical algorithms. Larsen [49] has noticed that when the kernels, $K^{(\Omega)}_{nlm}(r, \theta)$, are discretized this special functional form gives rise to a kernel matrix with block Kroneker product structure which can be used in a fast matrix-vector multiplication algorithm, and applied an iterative Lanczos-type algorithm to the inverse problem. This has made it possible to use the full 2dSOLA method even for the large SOI-MDI data sets.

Other ways of making localized averages more tractable for the two-dimensional problem include the $\mathbb{R}^1 \otimes \mathbb{R}^1$ methods, originally proposed in [72,73], which use the separation of the kernels K_{nlm} as in Eq. (101). The 1d×1dOLA method [72,74] is similar to the two-dimensional optimally localized averaging method, in that the solution is based on explicit determination of appropriate inversion coefficients $a^{(\Omega)}_i(r_0, \theta_0)$. However, these are not sought in the full space. Instead, motivated by the near-factorization of the splitting kernels, it is assumed that

$$a^{(\Omega)}_i = \tilde{c}_{nl} \beta_{lm}, \tag{102}$$

where the inversion coefficients $\{\beta_{lm}\}$ are determined in such a way that the first term of the angular part of the averaging kernel is localized (the SOLA method has been used for this purpose). Then the (radial) inversion coefficients $\{\tilde{c}_{nl}\}$ are determined by optimizing a localization criterion in two dimensions including the second term in Eq. (101) [74]. A more general version of this approach was developed in [61].

As in all SOLA-type methods, the free parameters are resolution widths in radius and in latitude for the Gaussian target functions usually used, and error-weighting factors.

3.2.3. Regularized least-squares method

The regularized least-squares method was applied to the 2D inverse problem in [70]. The goal of this method is to obtain a smooth solution that fits the data rather than to construct well-localized averaging kernels. This solution is obtained by minimizing the following functional:

$$\sum_{i=1}^{M} \frac{1}{\sigma_i^2} \left[\int_0^R \int_0^\pi K_i \Omega(r,\theta)\, \mathrm{d}\theta\, \mathrm{d}r - d_i \right]^2 + \alpha_r \int_0^R \int_0^\pi f_r(r,\theta) \left(\frac{\partial^2 \Omega}{\partial r^2} \right)^2 \mathrm{d}\theta\, \mathrm{d}r + \alpha_\theta \int_0^R \int_0^\pi f_\theta(r,\theta) \left(\frac{\partial^2 \Omega}{\partial \theta^2} \right)^2 \mathrm{d}\theta\, \mathrm{d}r, \tag{103}$$

where d_i are the observed frequency splittings or splitting coefficients, K_i are the corresponding seismic kernels, σ_i are the error estimates of the data, and α_r and α_θ are the regularization parameters, and f_r and f_θ are some weight functions which can be used to regulate the degree of smoothing in different regions. The last two terms provide smoothing using the second-derivative constraints, which provided good results for artificial and real data [68,70].

3.3. Results

As an example, we present some recent results obtained from SOI-MDI data [68]. These data consist of splitting coefficients $a_j(n,l)$ (Eq. (83)) obtained from the 144-day MDI time series by J. Schou using method [67] for $j = 1,\ldots,36$ and $1 \leqslant l \leqslant 250$. The presentation of the data in terms of the splitting coefficients rather than frequency splitting of the individual modes improves the stability of the measurements and reduces the number of data points. However, this also reduces the angular resolution of the results of inversion. The total number of measurements in this data set was $M = 37366$. Fig. 7 shows a set of the averaging kernels for the three different inversion methods described in this section. As expected, the optimally localized averaging methods provide better localization than the regularized least-squares method.

Fig. 8 shows the results of inversion of an artificial data set. We note that the results by the RLS method are somewhat closer to the actual rotation rate in the polar region (near the vertical axis) than the results by the SOLA method. The SOLA result has been recently improved in [50] by modifying the target kernel function, $\mathcal{T}(r_0,\theta_0,r,\theta)$, as discussed in Section 3.2.2.

Fig. 9 shows the results of inversion of the SOI-MDI data by the two methods. The results are generally in good agreement in most of the area where good averaging kernels were obtained. However, the results differ in the high-latitude region. In particular, a prominent feature at (0.2, 0.95) in Fig. 9a, which can be interpreted as a ‘polar jet’ is barely visible in Fig. 9b. Therefore, obtaining reliable inversion results in this region and also in the shaded area is one of the main current goals of helioseismology. This can be achieved by obtaining more accurate measurements of rotational frequency splitting and improving inversion techniques.

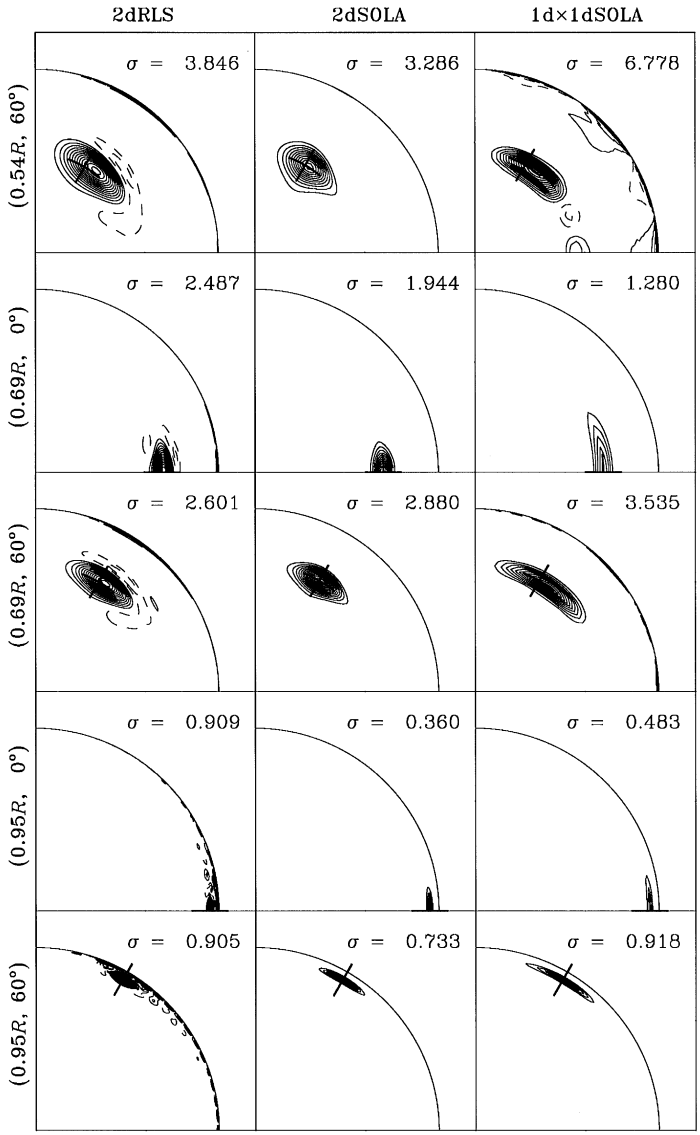

Fig. 7. Contour plots showing in a cross-section of the Sun a sample of the localized averaging kernels of 2D rotation inversions by the regularized least-squares (RLS) method and by two versions of the subtractive optimal localized averaging (SOLA) methods. The coordinates of the target points are shown along the left vertical axis, and indicated by crosses. The vertical axis is the polar axis, and the horizontal axis is an axis in the equatorial plane. The quarter of the circle indicates the solar surface at $r = R$. The standard error, σ, (in nHz) at each target point has been indicated (adopted from [68]).

4. Solar tomography

The basic idea of helioseismic tomography is to measure the acoustic travel time between different points on the solar surface, and then to use these measurement for inferring variations of the

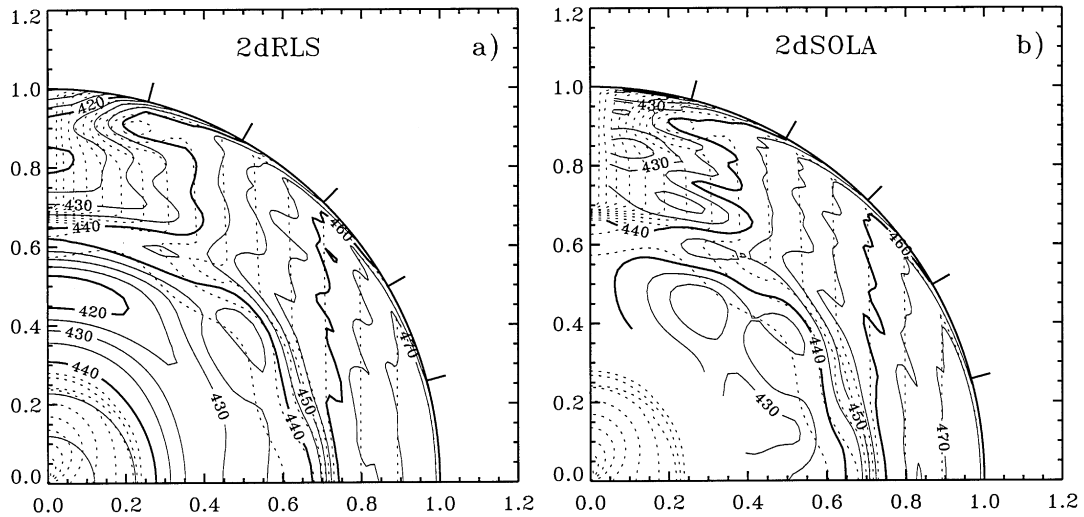

Fig. 8. Results of the test inversion by the RLS and SOLA methods. The dashed contour curves show the actual rotation (in nHz). The solid curves show the results of inversion of the test data perturbed with random Gaussian noise (adopted from [68]). The polar and equatorial axes are labeled with the relative radius.

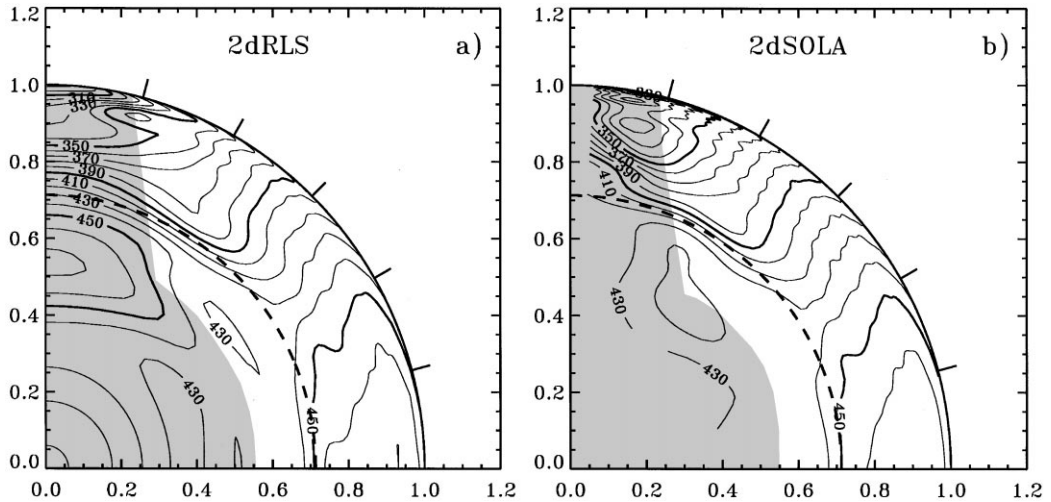

Fig. 9. Contour lines of the rotation rate (in nHz) inside the Sun obtained by inverting the rotational frequency splittings from a 144-day observing run from SOHO MDI by the RLS and SOLA methods. The shaded areas are the areas where the localized averaging kernels substantially deviate from the target positions (adopted from [68]).

structure and flow velocities in the interior along the wave paths connecting the surface points. This idea is similar to the Earth's seismology. However, unlike in Earth, the solar waves are generated stochastically by numerous acoustic sources in the subsurface layer of turbulent convection. Therefore, the wave travel times are determined from the cross-covariance function, $\Psi(\tau, \Delta)$, of the

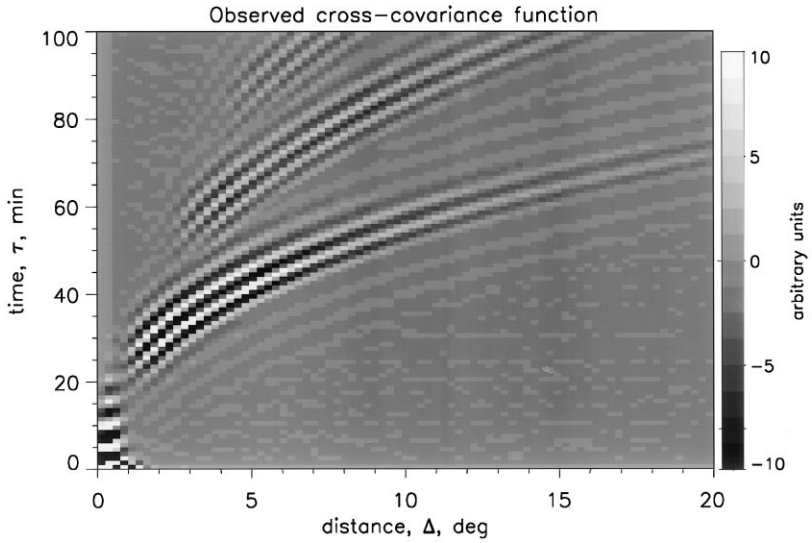

Fig. 10. The observed cross-covariance function as a function of distance on the solar surface, Δ, and the delay time, τ.

oscillation signal, $f(t,\boldsymbol{r})$, between different points on the solar surface [17]:

$$\Psi(\tau,\Delta)=\int_0^T f(t,\boldsymbol{r}_1)f^*(t+\tau,\boldsymbol{r}_2)\,\mathrm{d}t, \tag{104}$$

where Δ is the angular distance between the points with coordinates $\boldsymbol{r}_1$ and $\boldsymbol{r}_2$, τ is the delay time, and T is the total time of the observations. Because of the stochastic nature of excitation of the oscillations, function Ψ must be averaged over some areas on the solar surface to achieve a signal-to-noise ratio sufficient for measuring travel times τ. The oscillation signal, $f(t,\boldsymbol{r})$, is usually the Doppler velocity or intensity. A typical cross-covariance function shown in Fig. 10 displays three sets of ridges which correspond to the first, second and third bounces of acoustic wave packets from the surface [18].

The cross-covariance function represents a solar 'seismogram'. Ideally, the seismogram should be inverted to infer the structure and flows using a wave theory. However, in practice, as in terrestrial seismology [1] different approximations are employed, the most simple and powerful of which is the geometrical acoustic (ray) approximation. In the next section, we discuss relations between the modal wave approach and the ray theory [45].

4.1. Wave travel times and ray approximation

Generally, the observed solar oscillation signal corresponds to radial displacement or pressure perturbation, and can be represented in terms of normal modes, or standing waves (Section 2.1):

$$f(t,r,\theta,\phi)=\sum_{nlm} a_{nlm}\xi_{nlm}(r,\theta,\phi)\exp(\mathrm{i}\omega_{nlm}t+\mathrm{i}\phi_{nlm}), \tag{105}$$

where n,l and m are the radial order, angular degree and angular order of a normal mode, respectively, $\xi_{nlm}(r,\theta,\phi)$ is a mode eigenfunction in spherical coordinates, r,θ and ϕ,ω_{nlm} is the

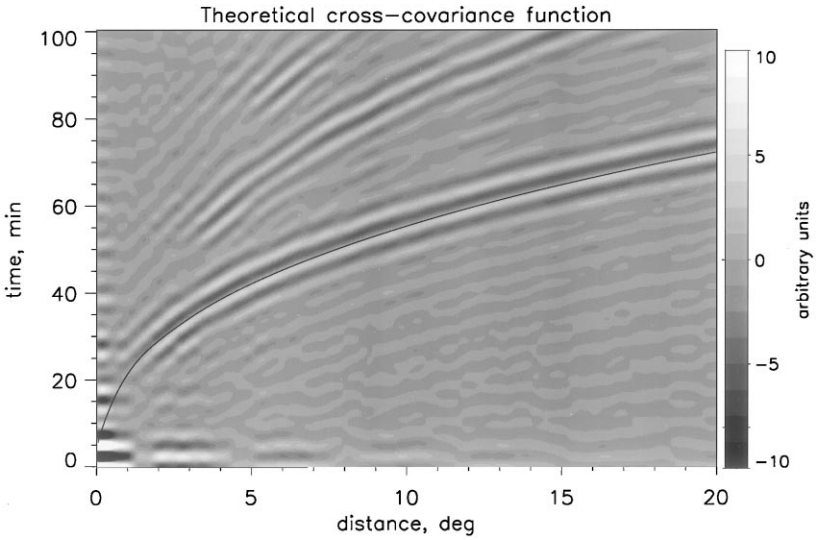

Fig. 11. The theoretical cross-covariance function of the solar p-modes of $l = 0$–1000 as a function of distance on the solar surface, Δ, and time, τ. The solid curve is the time–distance relation computed in the ray approximation (Eq. (107)).

eigenfrequency, and ϕ_{nlm} is an initial phase of the mode. Using Eq. (104), the cross-covariance function can be expressed in terms of normal modes, and then represented as a superposition of traveling wave packets. An example of the theoretical cross-covariance function of p modes of the standard solar model is shown in Fig. 11.

By grouping the modes in narrow ranges of the angular phase velocity, $v = \omega_{nl}/L$, where $L = \sqrt{l(l+1)}$, and applying the method of stationary phase, the cross-covariance function can be approximately represented in the form [45]

$$\Psi(\tau, \Delta) \propto \sum_{\delta v} \cos\left[\omega_0\left(\tau - \frac{\Delta}{v}\right)\right] \exp\left[-\frac{\delta\omega}{4}\left(\tau - \frac{\Delta}{u}\right)^2\right], \tag{106}$$

where δv is a narrow interval of the phase speed, $u \equiv (\partial\omega/\partial k_h)$ is the horizontal component of the group velocity, $k_h = 1/L$ is the angular component of the wave vector, and ω_0 is the central frequency of a Gaussian frequency filter applied to the data, and $\delta\omega$ is the characteristic width of this filter. Therefore, the phase and group travel times are measured by fitting individual terms of Eq. (106) to the observed cross-covariance function using a least-squares technique. In some cases, the ridges of the cross-covariance function may partially overlap, thus making the interpretation of the time–distance results more difficult [15].

This technique measures both phase (Δ/v) and group (Δ/u) travel times of the p-mode wave packets. The previous time–distance measurements provided either the group time [34], or an unspecified combination of the group and phase times [16]. It was found that the noise level in the phase-time measurements is substantially lower than in the group-time measurements. The geometrical acoustic (ray) approximation was employed to relate the measured phase times to the internal properties of the Sun. More precisely, the variations of the local travel times at different points on the surface, relative to the travel times averaged over the observed area are measured. Then variations of the

internal structure and flow velocities are inferred from the travel time anomalies using a perturbation theory.

In the ray approximation, the travel times are sensitive only to the perturbations along the ray paths given by

$$\frac{\mathrm{d}\boldsymbol{r}}{\mathrm{d}t}=\frac{\partial\omega}{\partial\boldsymbol{k}},\quad \frac{\mathrm{d}\boldsymbol{k}}{\mathrm{d}t}=\frac{\partial\omega}{\partial\boldsymbol{r}}, \tag{107}$$

where $\boldsymbol{r}$ is the radius-vector and $\boldsymbol{k}$ is the wave vector. The variations of the travel time obey Fermat's Principle (e.g. [25]):

$$\delta\tau=\frac{1}{\omega}\int_{\Gamma}\delta\boldsymbol{k}\cdot\mathrm{d}\boldsymbol{r}, \tag{108}$$

where $\delta\boldsymbol{k}$ is the perturbation of the wave vector due to the structural inhomogeneities and flows along the unperturbed ray path, Γ.

The dispersion relation for magnetoacoustic waves in the convection zone is

$$(\omega-\boldsymbol{k}\cdot\boldsymbol{U})^2=\omega_{\mathrm{c}}^2+k^2c_{\mathrm{f}}^2, \tag{109}$$

where $\boldsymbol{U}$ is the flow velocity, ω_{c} is the acoustic cut-off frequency,

$$c_{\mathrm{f}}^2=\tfrac{1}{2}(c^2+c_{\mathrm{A}}^2+\sqrt{(c^2+c_{\mathrm{A}}^2)^2-4c^2(\boldsymbol{k}\cdot\boldsymbol{c}_{\mathrm{A}})^2/k^2})$$

is the fast magnetoacoustic speed, $\boldsymbol{c}_{\mathrm{A}}=\boldsymbol{B}/\sqrt{4\pi\rho}$ is the vector Alfvén velocity, $\boldsymbol{B}$ is the magnetic field strength, c is the adiabatic sound speed, and ρ is the plasma density. If we assume that, in the unperturbed state $\boldsymbol{U}=\boldsymbol{B}=0$, then, to the first-order approximation

$$\delta\tau=-\int_{\Gamma}\left[\frac{(\boldsymbol{n}\cdot\boldsymbol{U})}{c^2}+\frac{\delta c}{c}S+\left(\frac{\delta\omega_{\mathrm{c}}}{\omega_{\mathrm{c}}}\right)\frac{\omega_{\mathrm{c}}^2}{\omega^2c^2S}+\frac{1}{2}\left(\frac{c_{\mathrm{A}}^2}{c^2}-\frac{(\boldsymbol{k}\cdot\boldsymbol{c}_{\mathrm{A}})^2}{k^2c^2}\right)S\right]\mathrm{d}s, \tag{110}$$

where $\boldsymbol{n}$ is a unit vector tangent to the ray, $S=k/\omega$ is the phase slowness. Then, we separate the effects of flows and structural perturbations by taking the difference and the mean of the reciprocal travel times:

$$\delta\tau_{\mathrm{diff}}=-2\int_{\Gamma}\frac{(\boldsymbol{n}\cdot\boldsymbol{U})}{c^2}\,\mathrm{d}s, \tag{111}$$

$$\delta\tau_{\mathrm{mean}}=-\int_{\Gamma}\left[\frac{\delta c}{c}S+\left(\frac{\delta\omega_{\mathrm{c}}}{\omega_{\mathrm{c}}}\right)\frac{\omega_{\mathrm{c}}^2}{\omega^2c^2S}+\frac{1}{2}\left(\frac{c_{\mathrm{A}}^2}{c^2}-\frac{(\boldsymbol{k}\cdot\boldsymbol{c}_{\mathrm{A}})^2}{k^2c^2}\right)S\right]\mathrm{d}s. \tag{112}$$

Anisotropy of the last term of Eq. (112) allows us to separate, at least partly, the magnetic effects from the variations of the sound speed and the acoustic cut-off frequency. The acoustic cut-off frequency, ω_{c} may be perturbed by the surface magnetic fields and by the temperature and density inhomogeneities. The effect of the cut-off frequency variation depends strongly on the wave frequency, and, therefore, it should result in frequency dependence in τ_{mean}. However, a significant frequency dependence in the observed travel times has not been detected yet.

Typically, the measurements represent times for acoustic waves to travel between points on the solar surface and surrounding quadrants symmetrical relative to the North, South, East and West directions. In each quadrant, the travel times are averaged over narrow ranges of travel distance Δ. Then, the times for northward-directed waves are subtracted from the times for south-directed waves

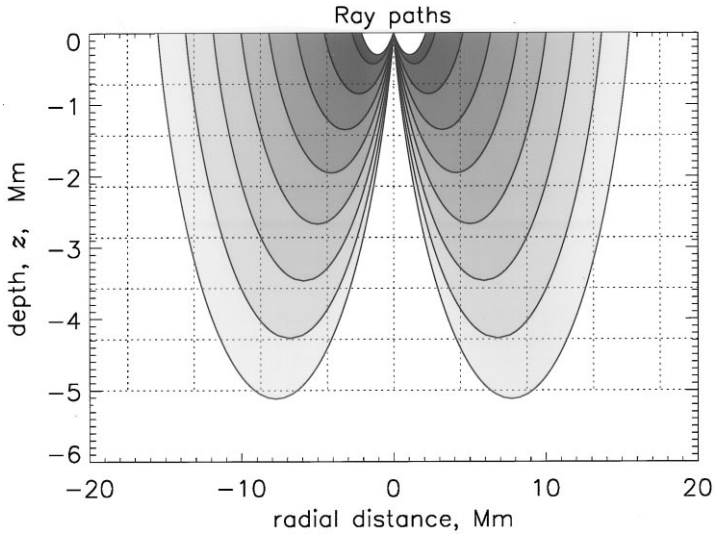

Fig. 12. The regions of ray propagation (shaded areas) as a function of depth, z, and the radial distance, Δ, from a point on the surface. The rays are also averaged over a circular region on the surface, forming three-dimensional figures of revolution. The dashed lines are the boundaries of the inversion grid.

to yield the time, $\tau_{\mathrm{diff}}^{\mathrm{NS}}$, which predominantly measures north–south motions. Similarly, the time differences, $\tau_{\mathrm{diff}}^{\mathrm{EW}}$, between westward- and eastward directed waves yields a measure of eastward motion. The time, $\tau_{\mathrm{diff}}^{\mathrm{oi}}$, between outward- and inward-directed waves, averaged over the full annuli, is mainly sensitive to vertical motion and the horizontal divergence.

4.2. Inversion method

It is assumed that the convective structures and flows do not change during the observations and can be represented by a discrete model. In this model, the 3-D region of wave propagation is divided into rectangular blocks. The perturbations of the sound speed and the three components of the flow velocity are approximated by linear functions of coordinates within each block, e.g.

$$\boldsymbol{U}(x,y,z)=\sum \boldsymbol{C}_{ijk}\left[1-\frac{|x-x_i|}{x_{i+1}-x_i}\right]\left[1-\frac{|y-y_j|}{y_{j+1}-y_j}\right]\left[1-\frac{|z-z_k|}{z_{k+1}-z_k}\right], \tag{113}$$

where x_i, y_j, z_k are the coordinates of the rectangular grid, $\boldsymbol{C}_{ijk}$ are the values of the velocity in the grid points, and $x_i \leqslant x \leqslant x_{i+1}$, $y_j \leqslant y \leqslant y_{j+1}$, and $z_k \leqslant z \leqslant z_{k+1}$. A part of the $x-z$ grid is shown in Fig. 12 together with the ray system used in the inversions.

The travel time measured at a point on the solar surface is the result of the cumulative effects of the perturbations in each of the traversed rays of the 3D ray systems. Fig. 12 shows, in the ray approximation, the sensitivity to given subsurface location for a certain point on the surface. This pattern is then moved around for different surface points in the observed area, so that overall the data are sensitive to all subsurface points in the depth range 0–5 Mm.

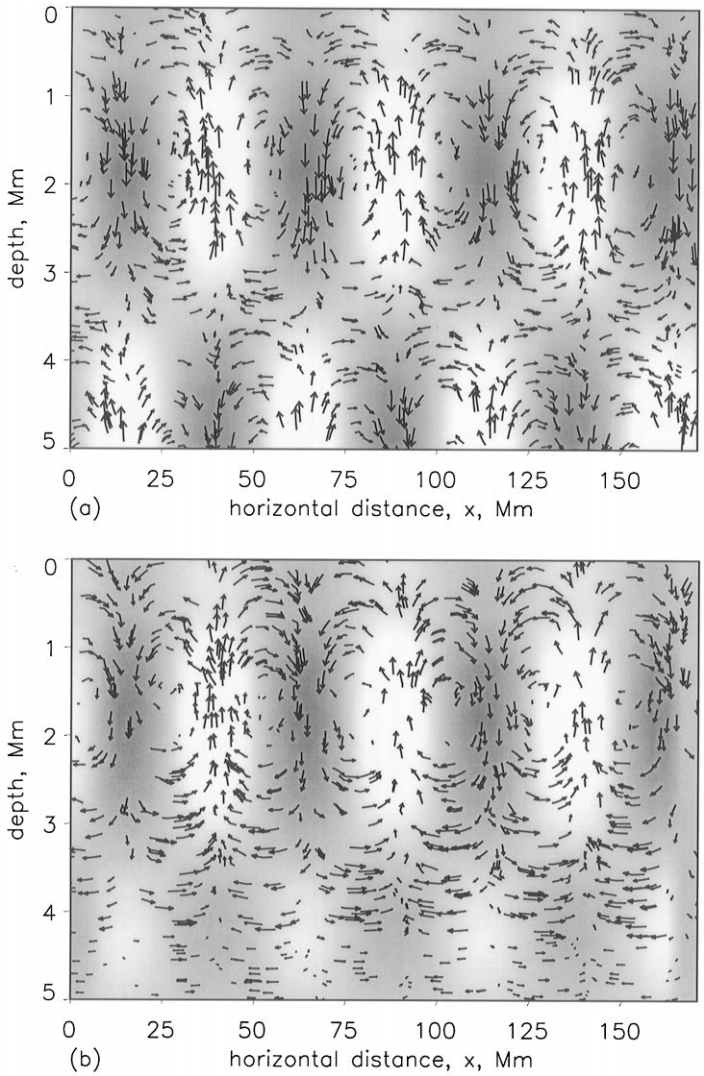

Fig. 13. (a) A vertical cut of the flow pattern (arrows) and the sound-speed perturbation (grey-scale background) in a test model of convection; (b) the result of inversion of the travel times computed for the system of rays shown in Fig. 12.

Therefore, Eqs. (110) and (112) are averaged over the ray systems corresponding to the different radial distance intervals of the data, using approximately the same number of ray paths as in the observational procedure. As a result, one obtains two systems of linear equations that relate the data to the sound speed variation and to the flow velocity, e.g. for the velocity field,

$$\delta\tau_{\mathrm{diff};\lambda\mu\nu} = \sum_{ijk} \boldsymbol{A}^{ijk}_{\lambda\mu\nu} \cdot \boldsymbol{C}_{ijk}, \tag{114}$$

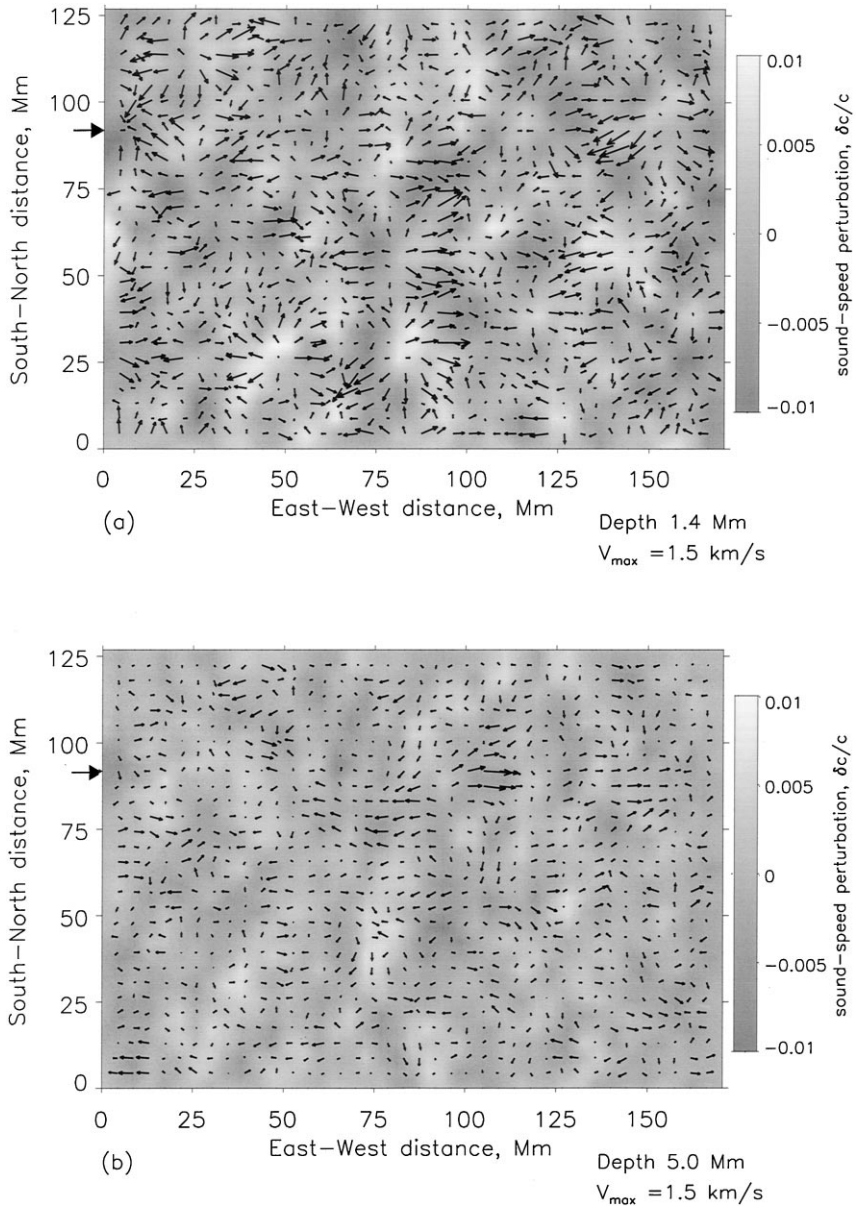

Fig. 14. The horizontal flow velocity field (arrows) and the sound-speed perturbation (grey-scale background) at the depths of 1.4 Mm (a) and 5.0 Mm (b), as inferred from the SOHO/MDI high-resolution data of 27 January 1996. The arrows at the south–north axis indicate the location of the vertical cut in the east–west direction, which is shown in Fig. 15.

where vector-matrix $\boldsymbol{A}$ maps the structure properties into the observed travel time variations, and indexes λ and μ label the location of the central point of a ray system on the surface, and index v labels surrounding annuli. These equations are solved by a regularized least-squares technique using

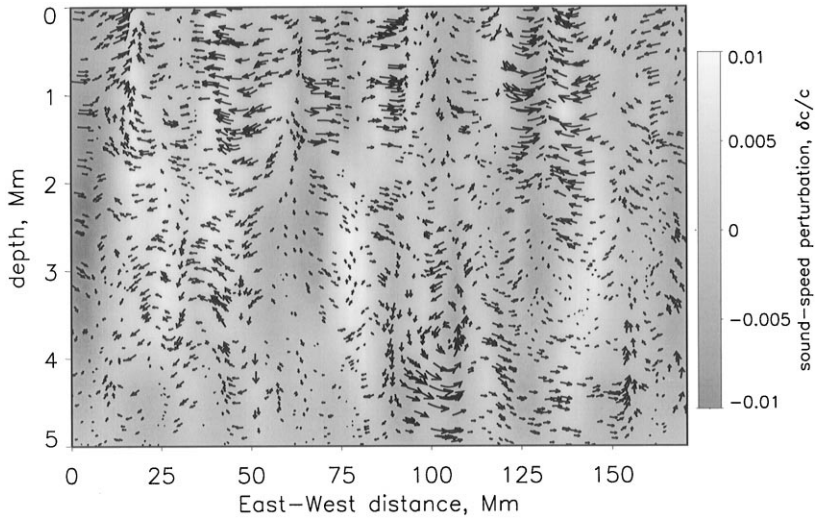

Fig. 15. The vertical flow field (arrows) and the sound-speed perturbation (grey-scale background) at the north–south position indicated by arrows in Fig. 14.

the LSQR algorithm [58]. In [35], it was suggested to speed up the inversion by doing most of the calculation in the Fourier domain.

The resolution and accuracy of the inversions were tested for an artificial model of multi-level convective flow [45]. The results of inversion of the test data in comparison with the original model are shown in Fig. 13. These results demonstrate a very accurate reconstruction of the horizontal components of the flow. However, the vertical flow in the deep layers is not resolved because of the predominantly horizontal propagation of the rays in these layers. The vertical velocities are also systematically underestimated by 10–20% in the upper layers.

4.3. Inversion results

Helioseismic tomography has been used to study local properties of large-scale zonal and meridional flows [24], convective flows and structures [18,45], structure and dynamics of active regions [42], flows around sunspots [16]. For illustration, we present here some results of tomographic inversions for large-scale convective cells (‘supergranulation’) and emerging active regions.

4.3.1. Quiet-Sun convection

Using the techniques of time-distance helioseismology, near-surface convective flows and structures using data from the SOI/MDI experiment on SOHO have been investigated [18,45]. The data used were for 8.5 h on January 27, 1996 from the high-resolution mode of the MDI instrument. The results of inversion of these data are shown in Figs. 14 and 15. It was found that, in the upper layers, 2–3 Mm deep, the horizontal flow is organized in supergranular cells, with outflows from the center of the supergranules. The characteristic size of the cells is 20–30 Mm. Comparing with

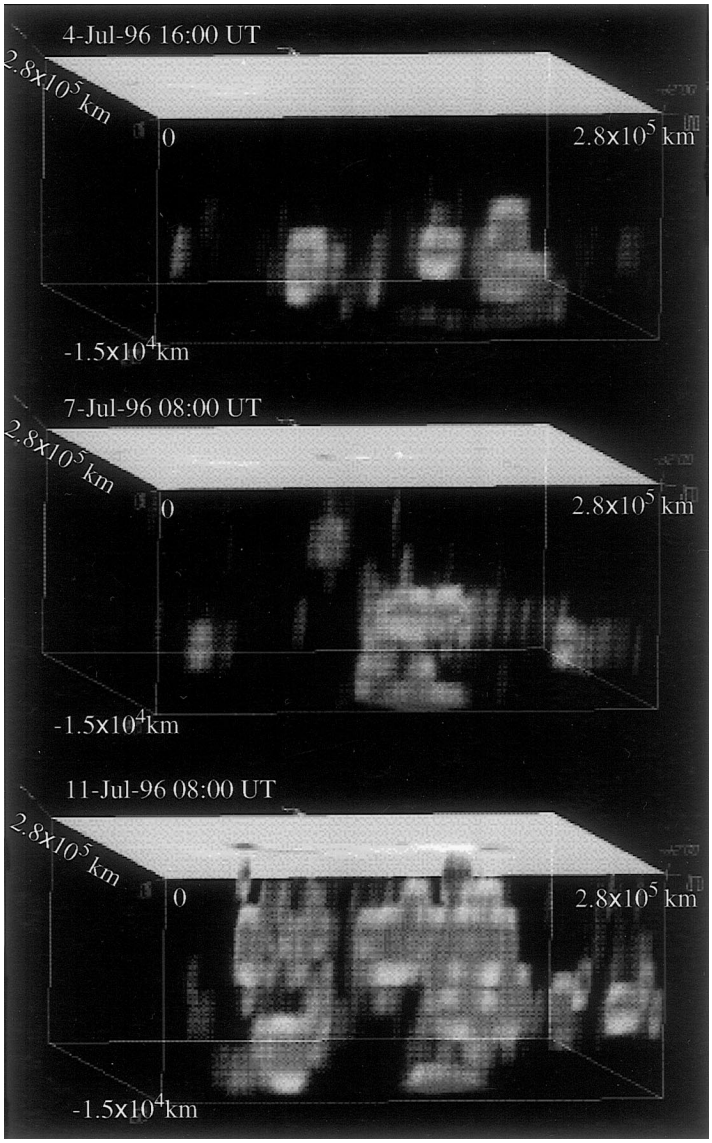

Fig. 16. Volume rendering of the sound-speed perturbation in the emerging active region NOAA 7879 on 4-Jul-96, 16:00 UT (top panel), 7-Jul-96, 8:00 (middle panel), and 11-Jul-96, 8:00 (bottom panel). The interior of the Sun is viewed from beneath. The panel on the top is à magnetogram showing the surface magnetic field of positive (white) and negative (black) polarities. The horizontal size of the box is approximately 280 Mm, the vertical size is 15 Mm. The perturbations of the sound speed which range from −1.5 to 1.5 km/s, are negative (dark grey) beneath the sunspots in the bottom panel, and positive (lighter grey) in other places (Electronic Annex available. See http://www.elsevier.nl/locate/cam).

MDI magnetograms, it was found that the cell boundaries coincide with the areas of enhanced magnetic field. The vertical flows (Fig. 15) correlate with the supergranular pattern in the upper layers. Typically, there are upflows in the ‘hotter’ areas where the sound speed is higher than average, and downflows in the ‘colder’ areas.

4.3.2. Tomography of emerging active regions

An important problem of astrophysics is understanding the mechanisms of solar activity. Helioseismic tomography provides a tool for studying the birth and evolution of active regions and complexities of solar activity [46]. Fig. 16 shows an example of the emerging active region of July 1996. The perturbations of the magnetosonic speed shown at three different periods are associated with the magnetic field and temperature variations in the emerging magnetic ropes. These perturbation are positive almost everywhere except in the regions beneath the sunspots in the bottom panel, probably, because of the lower temperature. However, the effects of temperature and magnetic field are not fully separated yet in these inversions. This is a very important problem of solar tomography.

5. Conclusion

Helioseismic inversions have provided unique information about the structure and dynamics of the solar interior. These inverse problems can be reduced to systems of linear integral equations to some degree of approximation, and, thus, can be solved, in principle, by standard inversion methods. However, taking into account specific features of these problems discussed in this paper allows us to develop more accurate and more efficient techniques. Helioseismology is a fairly new subject. During the first 10 years of its development substantial experience of solving the inverse problems has been accumulated. However, the methods for two- and three-dimensional problems are still in a very initial stage.

The methods for the first helioseismic inverse problem of determining the radial stratification, which is important for understanding solar and stellar evolution, have been developed in considerable detail (Section 2). The future efforts will focus on the diagnostics of the central energy-generating core ($r/R < 0.2$) and on the subsurface layers of turbulent convection. It is also important to develop 'super-resolution' methods for resolving the small-scale structures in the transition region between the radiative and convective zones (Fig. 6).

The inversion methods for inferring the internal rotation and the aspherical component of the solar structure (Section 3) are considerably less developed. These problems are two-dimensional and involve very large data sets (10^5–10^6 data points). This requires developing efficient numerical algorithms, the most successful of which employ the special (Kroneker-type) structure of the integral kernels. The most important problem of these inversions is developing new regularization methods which would allow a solution at high latitudes, close to the solar poles, and the solar core, – the regions shown in grey in Fig. 9. The potential of the 2D asymptotic inversion method (Section 3.2.1) has not been fully explored.

Solar tomography, or time–distance helioseismology, provides unique information about 3-D structures and flows associated with magnetic field and turbulent convection. This technique is at the very beginning of its development. In this paper, we have reviewed some basic principles of this technique based on the geometrical ray approximation, and initial inversion results. This method leads to fairly large least-squares problems currently solved using the LSQR iterative method. However, the validity of the ray approximation has not been established yet. Developing waveform solar tomography is one of the most challenging problems of computational helioseismology.

References

[1] K. Aki, P. Richards, Quantitative Seismology. Theory and Methods, Freeman, San Francisco, 1980.
[2] H.M. Antia, S. Basu, Nonasymptotic helioseismic inversion for solar structure, Astron. & Astrophys. Suppl. 107 (1994) 421–444.
[3] G.E. Backus, J.F. Gilbert, Numerical applications of a formalism for geophysical inverse problems, Geophys. J. Roy. Astron. Soc. 13 (1967) 247–276.
[4] G.E. Backus, J.F. Gilbert, The resolving power of gross earth data, Geophys. J. Roy. Astron. Soc. 16 (1968) 169–205.
[5] G.E. Backus, J.F. Gilbert, Uniqueness in the inversion of inaccurate gross earth data, Philos. Trans. Roy. Soc. London A 266 (1970) 123–192.
[6] J.N. Bahcall, M.H. Pinsonneault, Standard solar models, with and without helium diffusion, and the solar neutrino problem, Rev. Mod. Phys. 64 (1992) 885–926.
[7] S. Basu, H.M. Antia, D. Narasimha, Helioseismic measurement of the extent of overshoot below the solar convection zone, Mon. Not. Roy. Astron. Soc. 267 (1994) 209–224.
[8] M.A. Brodsky, A. Levshin, An asymptotic approach to the inversion of free oscillation data, Geophys. J. Roy. Astron. Soc. 58 (1979) 631–654.
[9] T.M. Brown, J. Christensen-Dalsgaard, W.A. Dziembowski, P. Goode, D.O. Gough, C.A. Morrow, Sun's internal angular velocity from observed p-mode frequency splittings, Astrophys. J. 343 (1989) 526–546.
[10] S. Chandrasekhar, A general variational principle governing the radial and the nonradial oscillations of gaseous masses, Astrophys. J. 138 (1963) 896–897.
[11] J. Christensen-Dalsgaard, D.O. Gough, M.J. Thompson, The depth of the solar convection zone, Astrophys. J. 378 (1991) 413–437.
[12] J. Christensen-Dalsgaard, W. Däppen, S.V. Ajukov, E.R. Anderson, H.M. Antia, S. Basu, V.A. Baturin, G. Berthomieu, B. Chaboyer, S. M. Chitre, A.N. Cox, P. Demarque, J. Donatowicz, W. A. Dziembowski, M. Gabriel, D.O. Gough, D.B. Guenther, J.A. Guzik, J.W. Harvey, F. Hill, G. Houdek, C.A. Iglesias, A.G. Kosovichev, J.W. Leibacher, P. Morel, C.R. Proffitt, J. Provost, J. Reiter, E.J. Rhodes Jr., F.J. Rogers, I.W. Roxburgh, M.J. Thompson, R.K. Ulrich, The current state of solar modeling, Science 272 (1996) 1286–1292.
[13] J.P. Cox, Theory of Stellar Pulsation, Princeton University Press, Princeton, 1980.
[14] W. Däppen, D.O. Gough, A.G. Kosovichev, M.J. Thompson, A new inversion for the hydrostatic stratification of the Sun, in: D.O. Gough, J. Toomre (Eds.), Challenges to Theories of the Structure of Moderate-Mass Stars, Springer, Heidelberg, 1991, pp. 111–120.
[15] S. D'Silva, Computing travel time in time-distance helioseismology, Astrophys. J. 498 (1988) L79–L82.
[16] T.L. Duvall Jr., S. D'Silva, S.M. Jefferies, J.W. Harvey, J. Schou, Downflows under sunspots detected by helioseismic tomography, Nature 379 (1996) 235–237.
[17] T.L. Duvall Jr., S.M. Jefferies, J.W. Harvey, M.A. Pomerantz, Time-distance helioseismology, Nature 362 (1993) 430–432.
[18] T.L. Duvall Jr., A.G. Kosovichev, P.H. Scherrer, R.S. Bogart, R.I. Bush, C. De Forest, J.T. Hoeksema, J. Schou, J.L.R. Saba, T.D. Tarbell, A.M. Title, C.J. Wolfson, P.N. Milford, Time-distance seismology with the MDI instrument: initial results, Solar Phys. 170 (1997) 63–73.
[19] W.A. Dziembowski, P.H. Goode, Seismic sounding of the solar core: purging the corruption from the Sun's magnetic activity, Astron. & Astrophys. 317 (1997) 919–924.
[20] W.A. Dziembowski, A.A. Pamjatnykh, R. Sienkiewicz, Solar model from helioseismology and the neutrino flux problem, Mon. Not. Roy. Astron. Soc. 244 (1990) 542–550.
[21] J.R. Elliott, Opacity determination in the solar interior, Mon. Not. Roy. Astron. Soc. 277 (1995) 1567–1579.
[22] J.R. Elliott, Equation of state in the solar convection zone and the implications of helioseismology, Mon. Not. Roy. Astron. Soc. 280 (1996) 1244–1256.
[23] J.R. Elliott, A.G. Kosovichev, The adiabatic exponent in the solar core, Astrophys. J. 500 (1998) L199–L202.
[24] P.M. Giles, T.L. Duvall Jr., P.H. Scherrer, Time-distance measurements of subsurface rotation and meridional flow, in: S.G. Korzennik, A. Wilson (Eds.), Structure and Dynamics of the Interior of the Sun and Sun-like Stars, ESA Publication, Noordwijk, 1998, 775–780.
[25] D.O. Gough, Linear adiabatic stellar pulsation, in: J.-P. Zahn, J. Zinn-Justin (Eds.), Astrophysical Fluid Dynamics, Elsevier Science Publ., Amsterdam, 1993, pp. 339.

[26] D.O. Gough, A.G. Kosovichev, An attempt to understand the Stanford p-mode data, in: E.J. Rolfe (Ed.), Seismology of the Sun and Sun-Like Stars, ESA SP-286, Noordwijk, 1988, pp. 195–201.
[27] D.O. Gough, A.G. Kosovichev, Using helioseismic data to probe the hydrogen abundance in the solar core, in: G. Berthomieu, M. Cribier (Eds.), Inside the Sun, Kluwer, Dordrecht, 1990, pp. 327–340.
[28] D.O. Gough, A.G. Kosovichev, Seismic effects of north-south asymmetry of Sun's rotation, in: R.K. Ulrich, E.J. Rhodes Jr., W. Däppen (Eds.), Gong '94: Helio- and Astero-Seismology from the Earth and Space, Astronomical Society of the Pacific, San Francisco, 1994, pp. 63–66.
[29] D.O. Gough, A.G. Kosovichev, J. Toomre, E. Anderson, H.M. Antia, S. Basu, B. Chaboyer, S.M. Chitre, J. Christensen-Dalsgaard, W.A. Dziembowski, A. Eff-Darwich, J.R. Elliott, P. Giles, P.R. Goode, J.A. Guzik, J.W. Harvey, F. Hill, J.W. Leibacher, M.J.P.F.G. Monteiro, O. Richard, T. Sekii, H. Shibahashi, M. Takata, M.J. Thompson, S. Vauclair, S.V. Vorontsov, The seismic structure of the sun, Science 272 (1996) 1296–1300.
[30] D.O. Gough, M.J. Thompson, The inversion problem, in: A.N. Cox, W.C. Livingston, M.S. Matthews (Eds.), Solar Interior and Atmosphere, Univ. Arizona Press, Tucson, 1991, pp. 519–561.
[31] D.O. Gough, J. Toomre, Seismic observations of the solar interior, Ann. Rev. Astron. Astrophys. 29 (1991) 627–685.
[32] J.W. Harvey, F. Hill, R.P. Hubbard, J.R. Kennedy, J.W. Leibacher, J.A. Pintar, P.A. Gilman, R.W. Noyes, A.M. Title, J. Toomre, R.K. Ulrich, A. Bhatnagar, J.A. Kennewell, W. Marquette, J. Patrón, O. Saá, E. Yasukawa, The Global Oscillation Network Group (GONG) Project, Science 272 (1996) 1284–1286.
[33] F. Hill, P.B. Stark, R.T. Stebbins, E.R. Anderson, H.M. Antia, T.M. Brown, T.L. Duvall Jr., D.A. Haber, J.W. Harvey, D.H. Hathaway, R. Howe, R.P. Hubbard, H.P. Jones, J.R. Kennedy, S.G. Korzennik, A.G. Kosovichev, J.W. Leibacher, K.G. Libbrecht, J.A. Pintar, E.J. Rhodes Jr., J. Schou, M.J. Thompson, S. Tomczyk, C.G. Toner, R. Toussaint, W.E. Williams, The solar acoustic spectrum and eigenmode parameters, Science 272 (1996) 1292–1295.
[34] S.M. Jefferies, Y. Osaki, H. Shibahashi, T.L. Duvall Jr., J.W. Harvey, M.A. Pomerantz, Use of acoustic wave travel-time measurements to probe the near-surface layers of the Sun, Astrophys. J. 434 (1994) 795–800.
[35] J.M. Jensen, B.H. Jacobsen, J. Christensen-Dalsgaard, Rapid exact linearized inversion of time-distance helioseismic data in the periodic approximation, Proc. Interdisciplinary Inversion Workshop 5, Aarhus, 1997, pp. 57–67.
[36] A.G. Kosovichev, Solution of an inverse helioseismological problem from observations of solar gravitational oscillations, Bull. Crimean Astron. Obs. 75 (1986) 36–42.
[37] A.G. Kosovichev, Determination of the solar sound speed by an asymptotic inversion technique, in: E.J.Rolfe (Ed.), Seismology of the Sun and Sun-Like Stars, ESA SP-286, Noordwijk, 1988, pp. 533–537.
[38] A.G. Kosovichev, Determination of the internal rotation of the Sun from the frequency splitting of acoustic modes, Bull. Crimean Astrophys. Obs. 80 (1988) 167–179.
[39] A.G. Kosovichev, Structure of the solar core inferred from inversion of the frequencies of low-degree p-modes, in: Y.Osaki, H. Shibahashi (Eds.), Proc. OJI Seminar, Progress in Seismology of the Sun and Stars, Springer, Heidelberg, 1990, pp. 319–324.
[40] A.G. Kosovichev, Solar structure inversion package, SOI-TN-084, Stanford-Lockheed Inst. for Astrophysics and Space Research, Stanford, 1992.
[41] A.G. Kosovichev, Seismic measurements of the helium abundance and the depth of stellar convection zones, Mon. Not. Roy. Astron. Soc. 265 (1993) 1053–1056.
[42] A.G. Kosovichev, Tomographic imaging of the Suns interior, Astrophys. J. 461 (1996) L55–L57.
[43] A.G. Kosovichev, Helioseismic constraints on the gradient of angular velocity at the base of the solar convection zone, Astrophys. J. Lett. 469 (1996) L61–64.
[44] A.G. Kosovichev, J. Christensen-Dalsgaard, W. Däppen, W. A. Dziembowski, D.O. Gough, M.J. Thompson, Sources of uncertainty in direct seismological measurements of the solar helium abundance, Mon. Not. Roy. Astron. Soc. 259 (1992) 536–558.
[45] A.G. Kosovichev, T.L. Duvall Jr., Acoustic tomography of solar convective flows and structures, in: F.P. Pijpers, J. Christensen-Dalsgaard, C.S. Rosenthal (Eds.), SCORe'96: Solar Convection and Oscillations and their Relationship, Kluwer Academic Publishers, Dordrecht, 1997, pp. 241–260.
[46] A.G. Kosovichev, T.L. Duvall Jr., P.H. Scherrer, Time-distance helioseismology, Adv. Space Res. (1999) in press.
[47] A.G. Kosovichev, K.V. Parchevsky, An asymptotic solution of the inverse problem of helioseismology for the internal differential rotation of the Sun, Sov. Astron. Lett. 44 (1988) 201–204.

[48] A.G. Kosovichev, J. Schou, P.H. Scherrer, J. Aloise, L. Bacon, R.S. Bogart, R.I. Bush, C. De Forest, P.M. Giles, J.T. Hoeksema, R. Nigam, M. Rubin, S. Basu, J. Christensen-Dalsgaard, T.L. Duvall Jr., M.J. Thompson, D.O. Gough, E.J. Rhodes, J. Toomre, T.D. Tarbell, A.M. Title, D. Mathur, M. Morrison, C.J. Wolfson, I. Zayer, Structure and rotation of the solar interior: first results from the MDI medium-l program, Solar Phys. 170 (1997) 43–61.
[49] R.M. Larsen, Iterative algorithms for two-dimensional helioseismic inversions, in: B.H. Jacobson (Ed.), Methodology and Applications in Geophysics, Astronomy, Geodesy and Physics, Aarhus University, Aarhus, 1997, pp. 123–137.
[50] R.M. Larsen, J. Christensen-Dalsgaard, A.G. Kosovichev, J. Schou, Improved SOLA inversions of MDI data, in: S.G. Korzennik, A. Wilson (Eds.), Structure and Dynamics of the Interior of the Sun and Sun-like Stars, ESA Publication, Noordwijk, 1998, 813–818.
[51] R.M. Larsen, P.C. Hansen, Efficient implementation of the SOLO mollifier Method, Astron. & Astrophys. Suppl. 121 (1997) 587–598.
[52] A.K. Louis, P. Maass, A mollifier method for linear operator equations of the first kind, Inverse Problems 6 (1990) 427–440.
[53] D. Lynden-Bell, J.P. Ostriker, On the stability of differentially rotating bodies, Mon. Not. Roy. Astron. Soc. 136 (1967) 293–310.
[54] G.I. Marchuk, Methods of Numerical Mathematics, Springer, New York, 1975.
[55] D.M. Mihalas, W. Däppen, D.G. Hummer, The equation of state for stellar envelopes. II. Algorithm and selected results, Astrophys. J. 331 (1988) 815–825.
[56] A.B. Migdal, Approximation Methods in Quantum Mechanics, W.A. Benjamin, New York, 1969.
[57] M.J.P.F.G. Monteiro, J. Christensen-Dalsgaard, M.J. Thompson, Seismic study of overshoot at the base of the solar convective envelope, Astron. & Astrophys. 282 (1994) 247–262.
[58] C.C. Paige, M.A. Saunders, LSQR: an algorithm for sparse linear equations and sparse least squares, ACM Trans. Math. Software 8 (1982) 43–71.
[59] F.P. Pijpers, Solar rotation inversions and the relationship between a-coefficients and mode splittings, Astron. & Astrophys. 326 (1997) 1235–1240.
[60] F.P. Pijpers, M.J. Thompson, Faster formulations of the optimally localized averages method for helioseismic inversions, Astron. Astrophys. 262 (1992) L33–36.
[61] F.P. Pijpers, M.J. Thompson, A modified $\mathbb{R}^1 \otimes \mathbb{R}^1$ method for helioseismic rotation inversion, Mon. Not. Roy. Astron. Soc. 262 (1996) 498–510.
[62] C.R. Proffitt, G. Michaud, Gravitational settling in solar models, Astrophys. J. 380 (1991) 238–250.
[63] E.J. Rhodes Jr., A.G. Kosovichev, J. Schou, P.H. Scherrer, J. Reiter, Measurements of frequencies of solar oscillations from the MDI medium-l program, Solar Phys. 175 (1997) 287–310.
[64] F.J. Rogers, C.A. Iglesias, Radiative atomic Rosseland mean opacity tables, Astrophys. J. Suppl. Ser. 79 (1992) 507–568.
[65] F.J. Rogers, F.J. Swenson, C.A. Iglesias, OPAL equation-of-state tables for astrophysical applications, Astrophys. J. 456 (1996) 902–908.
[66] P.H. Scherrer, R.S. Bogart, R.I. Bush, J.T. Hoeksema, A.G. Kosovichev, J. Schou, W. Rosenberg, L. Springer, T.D. Tarbell, A.M. Title, C.J. Wolfson, I. Zayer, and the MDI Engineering Team, The Solar Oscillation Investigation — Michelson Doppler Imager, Solar Phys. 162 (1995) 129–188.
[67] J. Schou, On the analysis of helioseismic data, Thesis, Aarhus University, Aarhus, 1992.
[68] J. Schou, H.M. Antia, S. Basu, R.S. Bogart, R.I. Bush, S.M. Chitre, J. Christensen-Dalsgaard, M.P. Di Mauro, W.A. Dziembowski, A. Eff-Darwich, D.O. Gough, D.A. Haber, J.T. Hoeksema, R. Howe, S.G. Korzennik, A.G. Kosovichev, R.M. Larsen, F.P. Pijpers, P.H. Scherrer, T. Sekii, T.D. Tarbell, A.M. Title, M.J. Thompson, J. Toomre, Helioseismic studies with SOI-MDI of differential rotation in the solar envelope, Astrophys. J. 505 (1998) 390–417.
[69] J. Schou, R. Bogart, Flows and horizontal displacements from ring diagrams, Astrophys. J. 504 (1998) L131–L134.
[70] J. Schou, J. Christensen-Dalsgaard, M.J. Thompson, On comparing helioseismic two-dimensional inversion methods, Astrophys. J. 433 (1994) 389–416.
[71] J. Schou, A.G. Kosovichev, P.R. Goode, W.A. Dziembowski, Determination of the sun's seismic radius from the SOHO Michelson doppler imager, Astrophys. J. 489 (1997) L197–L200.
[72] T. Sekii, On the $\mathbb{R}^1 \otimes \mathbb{R}^1$ inversion technique for solar rotation, in: T.M. Brown (Ed.), Seismic Investigation of the Sun and Stars, ASP, San Francisco, 1993, pp. 237–240.

[73] T. Sekii, A new strategy for 2D inversion for solar rotation, Mon. Not. Roy. Astron. Soc. 264 (1993) 1018–1024.
[74] T. Sekii, The $\mathbb{R}^1 \otimes \mathbb{R}^1$ rotation inversion with expansion coefficients, in: J.T. Hoeksema et al. (Eds.), Proc. 4th SOHO Workshop, Helioseismology, Vol. 2, ESA, Noordwijk, 1995, pp. 285–288.
[75] M.J. Thompson, Helioseismic inversion, in: D.O. Gough, J. Toomre (Eds.), Challenges to Theories of the Structure of Moderate-Mass Stars, Springer, Heidelberg, 1991, pp. 61–80.
[76] M.J. Thompson, Seismic investigation of the sun's internal structure and rotation, in: T.M. Brown (Ed.), Seismic Investigation of the Sun and Stars, ASP, San Francisco, 1993, pp. 141–154.
[77] A.N. Tikhonov, V.Y. Arsenin, Solutions of Ill-Posed Problems, Winston, Washington, New York, 1977.
[78] W. Unno, Y. Osaki, H. Ando, H. Saio, H. Shibahashi, Nonradial Oscillations of Stars, University of Tokyo Press, Tokyo, 1989.